

Research Articles: Systems/Circuits

Excitatory projections from the prefrontal cortex to nucleus accumbens core D1-MSNs and kappa opioid receptor modulate itch-related scratching behaviors

<https://doi.org/10.1523/JNEUROSCI.1359-22.2023>

Cite as: J. Neurosci 2023; 10.1523/JNEUROSCI.1359-22.2023

Received: 11 July 2022

Revised: 28 December 2022

Accepted: 6 January 2023

This Early Release article has been peer-reviewed and accepted, but has not been through the composition and copyediting processes. The final version may differ slightly in style or formatting and will contain links to any extended data.

Alerts: Sign up at www.jneurosci.org/alerts to receive customized email alerts when the fully formatted version of this article is published.

1 **Excitatory projections from the prefrontal cortex to nucleus accumbens core D1-MSNs and kappa**
2 **opioid receptor modulate itch-related scratching behaviors**

3 Xiao-Bo Wu,* Qian Zhu, Ming-Hui Gao, Sheng-Xiang Yan, Pan-Yang Gu, Peng-Fei Zhang, Meng-Lin
4 Xu, Yong-Jing Gao*

5 Institute of Pain Medicine and Special Environmental Medicine, Co-innovation Center of
6 Neuroregeneration, Nantong University, Jiangsu 226019, China

7

8 Running title: mPFC-NAc core projection and acute itch

9 Number of words in Abstract: 249; Introduction: 518; Discussion: 1499

10 Number of figures: 9

11

12 *Correspondence:

13 Yong-Jing Gao, Institute of Pain Medicine, Nantong University, 9 Seyuan Road, Nantong, Jiangsu 226019,
14 China. Tel: +86-513-55003374; Email: gaoyongjing@ntu.edu.cn

15 Xiao-Bo Wu, Institute of Pain Medicine, Nantong University, 9 Seyuan Road, Nantong, Jiangsu 226019,
16 China. Tel: +86-513-55003373; Email: xbwu1983@ntu.edu.cn

17

18 **Acknowledgements**

19 This work was supported by STI2030-Major Projects 2022ZD0204700 and the National Natural Science
20 Foundation of China (NSFC Nos. 32030048 and 32171000).

21

22 **Conflict of interest statement**

23 The authors declare no competing financial interests.

24 **Abstract**

25 Itch is an uncomfortable and complex sensation that elicits the desire to scratch. The nucleus accumbens
26 (NAc) activity is important in driving sensation, motivation, and emotion. Excitatory afferents from the
27 medial prefrontal cortex (mPFC), amygdala, and hippocampus are crucial in tuning the activity of
28 dopamine receptor D1- and D2-expressing medium spiny neurons (Drd1- and Drd2-MSNs) in the NAc.
29 However, a cell-type and neural circuitry-based mechanism of the NAc underlying acute itch remains
30 unclear. We found that acute itch induced by compound 48/80 (C48/80) decreased the intrinsic membrane
31 excitability in Drd1-MSNs, but not in Drd2-MSNs in the NAc core of male mice. Chemogenetic
32 activation of Drd1-MSNs alleviated C48/80-induced scratching behaviors, but not itch-related anxiety-
33 like behaviors. In addition, C48/80 enhanced the frequency of spontaneous excitatory postsynaptic
34 currents (sEPSCs) and reduced the paired-pulse ratio of electrical stimulation-evoked EPSCs in Drd1-
35 MSNs. Furthermore, C48/80 increased excitatory synaptic afferents to Drd1-MSNs from the mPFC, not
36 from the basolateral amygdala or ventral hippocampus. Consistently, the intrinsic excitability of mPFC-
37 NAc projecting pyramidal neurons was increased after C48/80 treatment. Chemogenetic inhibition of
38 mPFC-NAc excitatory synaptic afferents relieved the scratching behaviors. Moreover, pharmacological
39 activation of kappa opioid receptor (KOR) in the NAc core suppressed C48/80-induced scratching
40 behaviors, and the modulation of KOR activity in the NAc resulted in the changes of presynaptic
41 excitatory inputs to Drd1-MSNs in C48/80-treated mice. Together, these results reveal the neural
42 plasticity in synapses of NAc Drd1-MSNs from the mPFC underlying acute itch and indicate the
43 modulatory role of the KOR in itch-related scratching behaviors.

44

45 **Key words:** medial prefrontal cortex; dopamine D1 receptor; medium spiny neurons; nucleus accumbens;
46 kappa opioid receptor; itch

47

48

49

50 **Significance Statement**

51 Itch stimuli cause strongly scratching desire and anxiety in patients. However, the related neural
52 mechanisms remain largely unclear. In the present study, we demonstrated that the pruritogen compound
53 48/80 (C48/80) shapes the excitability of dopamine receptor D1-expressing medium spiny neurons (Drd1-
54 MSNs) in the NAc core and the glutamatergic synaptic afferents from medial prefrontal cortex (mPFC) to
55 these neurons. Chemogenetic activation of Drd1-MSNs or inhibition of mPFC-NAc excitatory synaptic
56 afferents relieves the scratching behaviors. In addition, pharmacological activation of kappa opioid
57 receptor (KOR) in the NAc core alleviates C48/80-induced itch. Thus, targeting mPFC-NAc Drd1-MSNs
58 or KOR may provide effective treatments for itch.

59

60

61

62

63

64

65

66

67

68

69

70

71

72

73

74

75

76 **Introduction**

77 Itch is a complex and uncomfortable sensation that strongly provokes the desire to scratch. Repeated,
78 excessive scratches cause severe damage to the skin tissue and diminish the quality of life in patients with
79 chronic itch (Murota et al., 2010; Zachariae et al., 2012; Lavery et al., 2016). Human imaging studies
80 showed that scratching is related to the activity of the reward system, including the prefrontal cortex,
81 orbitofrontal cortex, midbrain, and caudate nucleus (Papoiu et al., 2013; Mochizuki et al., 2014;
82 Mochizuki et al., 2015). However, itching also triggers negative emotions like anxiety and depression
83 (Bartels et al., 2016; Sanders and Akiyama, 2018). Recent studies have identified that neuronal
84 populations in the amygdala are involved in itch-related sensation and negative emotions (Sanders et al.,
85 2019; Samineni et al., 2021). Additionally, the ventral tegmental area (VTA) dopaminergic neurons
86 process the itch-related scratching behavior, while GABAergic neurons are implicated in the itch-induced
87 aversion (Su et al., 2019).

88 The nucleus accumbens (NAc) is a critical brain region of mesolimbic dopamine circuitry and
89 roughly divided into the core and shell subregions (Zahm and Brog, 1992). The two subregions have
90 distinct anatomical structures and encode relatively different behaviors, but share similar local circuitry
91 (Floresco, 2015). NAc primarily receives excitatory afferents from the medial prefrontal cortex (mPFC),
92 basolateral amygdala (BLA), ventral hippocampus (vHipp), and thalamus that are involved in
93 motivation/desire-related behaviors (Suska et al., 2013; LeGates et al., 2018; Wang et al., 2020; Chisholm
94 et al., 2021). A recent study provide evidence that itch stimuli dynamically regulate dopamine level in the
95 NAc shell region, which is involved in itch-related scratching (Yuan et al., 2018; Yuan et al., 2019). In
96 addition, the anterior cingulate cortex and amygdala are activated by itch stimuli (Lu et al., 2018; Sanders
97 et al., 2019; Zhang et al., 2022). These results support the circuitry containing such brain regions may
98 contribute to the itch-related activities. Excitatory synaptic afferents integrate in the NAc medium-sized
99 spiny neurons (MSNs), which are transcriptionally segregated into dopamine D1 receptor-expressing
100 MSNs (Drd1-MSNs) and D2 receptor-expressing MSNs (Drd2-MSNs) (Kreitzer, 2009). Previous studies
101 demonstrated that different activities of Drd1- and Drd2-MSNs might code distinct emotional behavior

102 responses (Soares-Cunha et al., 2016). However, the neural circuits and functional roles of the NAc MSN
103 subtypes underlying itch-related scratching and affective components remain unknown.

104 In the NAc, the kappa opioid receptor (KOR) is densely expressed on the presynaptic terminals of
105 dopaminergic and glutamatergic inputs and regulates the release of dopamine and glutamate (Hjelmstad
106 and Fields, 2001; Karkhanis et al., 2016). Activation of KOR in the NAc modulates the response to
107 reward (Chartoff et al., 2016) and aversive stimuli, including pain-induced negative affect (Massaly et al.,
108 2019). Pharmacological studies have shown that KOR agonists are promising therapeutic candidates for
109 intractable itch by their antipruritic effects in both animals and humans (Phan et al., 2012). However, the
110 underlying mechanisms of the antipruritic effects for KOR activation remain elusive. In this study, we
111 investigated the role of MSN subtypes in the NAc core and their excitatory afferent circuits in itch-related
112 behaviors and provided the cellular evidence for KOR modulation on synaptic adaptation in itch signal
113 processing.

114

115 **Materials and Methods**

116 *Animals.* All animal procedures performed in this study were reviewed and approved by the Animal Care
117 and Use Committee of Nantong University (Jiangsu, China). Male mice (8 -12 weeks) were maintained
118 on a 12/12 hour of light/dark cycle (lights on at 6:30 A.M.) at room temperature of $22 \pm 3^\circ\text{C}$ with free
119 access to food and water. All mice were acclimated to the animal facility for 5-7 days prior to the
120 initiation of experimental procedures. *Drd1a-tdTomato* (6Calak/J, catalog #016204, The Jackson
121 Laboratory), *Drd2-EGFP* [B6.FVB(Cg)-Tg(Drd2-EGFP)S118Gsat/KreMmucd, catalog #036931-UCD,
122 MMRRC], and *Drd1a-Cre* (Tg(Drd1-cre)EY217Gsat/Mmcd, catalog #030778-UCD, MMRRC) BAC
123 transgenic mice on a C57BL/6J background were used in this study.

124

125 *Drugs.* U50488 was purchased from Tocris Bioscience. Compound 48/80 (C48/80), picrotoxin, clozapine
126 N-oxide (CNO), norbinaltorphimine (nor-BNI), and the other chemicals were purchased from Sigma-
127 Aldrich.

128

129 *Brain cannula implantation and drug injection.* The animals were anesthetized with isoflurane. Guided
130 cannulas (26 G, RWD Life Science, China) were implanted above the bilateral NAc (AP: + 1.5 mm;
131 lateral: ± 0.8 mm; depth: - 4.0 mm from the skull). An injection needle (32 G, Hamilton, United States)
132 was inserted through the guide cannula, and drug solution or vehicle (0.3 µl/site) was slowly injected over
133 5 min. Locations of the cannula placement were confirmed at the time of tissue harvest.

134

135 *Stereotaxic Surgery.* For optogenetic manipulation, the mice were anesthetized with isoflurane and
136 immobilized with a stereotaxic frame (RWD Life science, China). After a craniotomy was performed,
137 each mouse received a bilateral injection of pAAV9-CaMKII α -ChR2 (H134R)-eYFP (AAV-CaMKII α -
138 ChR2-eYFP, viral titer 5.2×10^{12} v.g./ml; packaged by Shanghai OBiO Technology) into the mPFC
139 (stereotaxic coordinates from Bregma: A/P: + 1.6 mm, M/L: ± 0.4 mm, D/V: - 2.5 mm), BLA (A/P: -1.3
140 mm, M/L: ± 2.8 mm, D/V: - 4.8 mm), or vHipp (A/P: - 3.1 mm, M/L: ± 2.9 mm, D/V: - 4.5 mm). A total
141 of 0.4-0.6 µl (two sites) of virus solution was infused at a rate of 0.05 µl/min by a syringe pump. The
142 amount of the injection volume is 0.6 µl (0.3 µl/site) into mPFC, 0.4 µl (0.2 µl/site) into BLA, and 0.6 µl
143 (0.3 µl/site) into vHipp. For chemogenetic manipulation, AAV5-Ef1 α -DIO-hM3D(Gq)-mCherry (AAV-
144 DIO-hM3Dq-mCherry), AAV5-Ef1 α -DIO-hM4D(Gi)-mCherry (AAV-DIO-hM4Di-mCherry), or AAV5-
145 Ef1 α -DIO-mCherry (AAV-DIO-mCherry) were bilaterally injected into the NAc core. For chemogenetic
146 inhibition of PFC-NAc synaptic projections, AAV5-CaMKII α -hM4D(Gi)-mCherry (AAV-CaMKII α -
147 hM4Di-mCherry) or AAV5-CaMKII α -mCherry (AAV-CaMKII α -mCherry) were bilaterally injected into
148 the mPFC (places are same as above), and then the cannulas were implanted into the NAc. After injection,
149 the syringe was left in place for 8-10 min. To identify PFC-NAc projection pyramidal neurons, 0.1 µl/site
150 retrobeads green was bilaterally injected into the NAc core (AP: + 1.5 mm; lateral: ± 0.8 mm; depth: - 4.2
151 mm from the skull).

152

153 *Neck model of acute itch.* All mice were shaved on the back of neck and then were habituated to the
154 experimenters by handling for 3 days before experiments. For the scratching behavior test, mice were
155 individually placed into small plastic chambers (15 × 15 × 15 cm) on an elevated metal mesh floor and
156 habituated for at least 30 min. After mild anesthesia with isoflurane, mice were injected intradermally
157 with Compound 48/80 (C48/80, 100 µg/50 µl; Sigma-Aldrich) or saline into the rostral back skin.
158 Immediately after the injection, the itch-related scratching behavior was recorded with a video camera for
159 30 min and the bouts of scratching were assessed. One bout of scratching was counted as a mouse lifting
160 of either hindpaw to scratch the injection site of the shaved skin and then returning it back to the floor or
161 licking/biting of the toes (Jing et al., 2018; Wu et al., 2021).

162
163 *Elevated plus-maze test.* The elevated plus-maze (EPM) test (EPMT) apparatus consisted of four arms (30
164 cm long and 5 cm wide) and was elevated 32 cm from the floor. All mice were acclimated to the testing
165 room 45 min before the initiation of the experiment. After intradermal injection of C48/80 or saline, each
166 mouse was placed back in the home cage for 30 min. After that, each mouse was placed at the center
167 square of the maze, facing the open arm, and allowed to explore the maze for 5 min. The entry into an
168 arm was counted by the presence of all four paws on the floor of that arm. The total time spent in the open
169 arms and the number of entries to these arms were used in the assessment of anxiety-like behavior. The
170 animal behavior parameters were analyzed with a video tracking and analysis system (ANY-maze
171 software, Stoelting, IL, USA). To eliminate the possible bias, all the arms were equally illuminated and
172 thoroughly cleaned with 75% ethanol after each trial.

173
174 *Open-field test.* The open-field (OF) test (OFT) apparatus is composed of a white PVC box (60 × 60 cm,
175 50 cm height). The floor was subdivided into 16 equal parts. The central zone was defined by the four
176 squares in the middle field. Same as in the EPM test, each mouse was acclimated to the testing room 45
177 min before the initiation of the experiment. After intradermal injection of C48/80 or saline, each mouse

178 was placed back in the home cage for 30 min. Then the mouse was put in the middle of the field and was
179 tested individually within a 5 min session. The behavioral data were analyzed by the ANY-maze system
180 (Stoelting Co., IL, USA). The time spent in the central zone and the total travel distance was counted. The
181 inner sides of the apparatus were carefully cleaned with 75% ethanol after each trial.

182

183 *Brain slices preparation and patch-clamp recording.* Brain slice preparation and whole-cell recordings
184 were conducted the same as our published protocol (Wu et al., 2018). Briefly, 30 min after saline or
185 C48/80 intradermal injection, the mice were anesthetized with isoflurane and decapitated. The brains
186 were quickly removed and immediately immersed into the ice-cold artificial cerebrospinal fluid (aCSF).
187 Sucrose-rich aCSF contains 235 mM sucrose, 2.5 mM KCl, 1.25 mM NaH₂PO₄, 1 mM CaCl₂, 2.5 mM
188 MgCl₂, 25 mM NaHCO₃, and 10 mM glucose, oxygenated with 95% O₂ plus 5% CO₂. Coronal brain
189 slices (250 μm) containing the NAc core or PFC region were cut with a vibratome (Series 1000; Leica,
190 Germany). Slices were incubated with oxygenated (95% O₂ + 5% CO₂) normal aCSF containing 125 mM
191 NaCl, 3 mM KCl, 1.25 mM NaH₂PO₄, 2.4 mM CaCl₂, 1.2 mM MgCl₂, 26 mM NaHCO₃, and 10 mM
192 glucose for 30 min at 34 °C and subsequently stored in room temperature at least 1 h before
193 electrophysiological recording.

194 Slices were placed in a recording chamber and were continuously perfused with oxygenated normal
195 aCSF. Cells were visualized by an infrared-differential interference contrast (IR-DIC) and fluorescent
196 microscope (BX51WIF, Olympus, Tokyo, Japan) equipped with a digital sCMOS camera (optiMOS,
197 QImaging, United States). Whole-cell patch-clamp recordings of NAc core neurons were conducted using
198 a patch-clamp amplifier (Multiclamp 700B; Molecular Devices, Burlingame, United States). Data
199 acquisition was performed by using a digitizer (DigiData 1400A; Molecular Devices, United States) and
200 analyzed with Clampfit 10.4 software (Molecular Devices, Sunnyvale, USA), respectively. Cells located
201 in the ventral-medial sub-region of the NAc core MSNs with tdTomato (Drd1+) or eGFP (Drd2+) were
202 identified by their fluorescence. A typical MSN was further confirmed by its small morphology (somatic
203 diameters, < 20 μm) and hyperpolarized resting membrane potential (hyperpolarize than -75 mV). For

204 PFC-NAc projection pyramidal neurons recording, retrobeads positive cells in the PFC region were
205 identified by their green fluorescence. The patch pipette resistance was 4-8 M Ω when filled with pipette
206 solution, and seal resistances were > 1 G Ω . Data were digitized at 10 kHz and low-pass filtered at 2 kHz.

207 The intrinsic membrane excitability recordings were performed with a pipette solution containing
208 120 mM K-gluconate, 20 mM KCl, 0.3 mM GTP-Tris, 4 mM Na₂ATP, 10 mM HEPES, 0.2 mM EGTA, 2
209 mM MgCl₂, pH 7.2-7.4, which adjusted with KOH. After establishing a well whole-cell configuration,
210 recordings were done in the current-clamp model at room temperature (23 \pm 1°C). All neuronal
211 excitability measurements were performed at the resting membrane potential (RMP). Only the RMP
212 “stable” (oscillating < 3 mV within 5 min) neurons were adopted for the following recordings. A series of
213 step currents (-200 to +200 pA, with a 20-pA increment, pulse duration, 1 sec, and inter-pulse interval, 15
214 s) were run (at least three runs) to measure the membrane properties. For a recorded neuron, the number
215 of evoked action potentials with a variation > 20 % (run-down or run-up) were excluded from further data
216 analysis.

217 To measure the EPSCs, electrodes were filled with a cesium-based internal pipette solution
218 containing 120 mM cesium methanesulfonate, 2 mM NaCl, 20 mM HEPES, 5 mM tetraethylammonium-
219 Cl, 0.4 mM EGTA, 2.5 mM Na₂ATP, 0.3 mM GTP-Tris, and 2.5 mM QX-314, pH 7.2-7.4, which
220 adjusted with CsOH. The spontaneous and evoked EPSCs were recorded at -70 mV in a voltage-clamp
221 model. Spontaneous EPSCs (sEPSCs) were obtained at least 10 min for each recorded cell and GABA_A
222 receptor antagonist picrotoxin (PTX, 100 μ M) was present in the aCSF. For sEPSCs analysis, a template
223 was conducted by averaging 80~100 hand-picked spontaneous events with pClamp10.4 software. To
224 measure the role of the kappa receptor in excitatory synaptic transmission at the NAc core, miniature
225 EPSCs (mEPSCs) were obtained in the presence of 100 μ M PTX and 1 μ M TTX. The selective KOR
226 agonist U50488 (1 μ M) or selective KOR antagonist nor-BNI (0.1 μ M) was added to the aCSF after the
227 basal recording (Mu et al., 2011; Kallupi et al., 2013). Electrical stimulations (produced by Master 8;
228 AMPI Technologies) at 0.1 Hz (pulse of 100 μ s duration) by a concentric bipolar electrode (FHC,

229 Bowdoinham, ME) were used to evoke EPSCs in some experiments. The stimulating electrode was
230 placed 150-200 μm rostral to the recording electrode. The intensity inducing the 60% of the maximum
231 amplitude of EPSC was adopted as the test stimulation, except for the experiment for conducting the
232 input-output (I-O) relationship of EPSCs. For each cell at each stimulus intensity tested, ~ 20 consecutive
233 EPSCs were recorded and the peak amplitudes were averaged. A series of inter-pulses interval times (25
234 ms, 50 ms, 100 ms, and 200 ms) was adopted in the paired-pulse ratio (PPR) test.

235 To stimulate specific synaptic inputs into NAc slices, a LED illumination (LAMBDA HPX-5, Sutter
236 Instrument, United States) coupled with a band pass excitation filter (470/40 nm) was used in the
237 experiment. Optical stimulation pulse (2 ms, 2~5 mW) was chosen for each cell recording. The GABA_A
238 receptor antagonist PTX (100 μM) was present in the aCSF throughout the experiment. The inter-pulses
239 interval time containing 50 ms, 100 ms, 200 ms, and 10 s was used in light stimulation evoked PPR test.
240 The AMPAR/NMDAR ratio was calculated by EPSCs (~ 20 consecutive traces) recorded at -70 mV and
241 then holding the cell to +40 mV and collecting another EPSCs (~ 20 consecutive traces). The averaged
242 EPSCs peak at -70 mV was measured as the AMPAR-mediated EPSC. The NMDAR-mediated EPSCs
243 were calculated by measuring the value of the averaged EPSCs (held at + 40 mV) after 50 to 55 ms of
244 light stimulation.

245

246 *Histology and imaging.* Animals were deeply anesthetized with isoflurane and perfused intracardially
247 with cold PBS followed by 4% paraformaldehyde (PFA). Brains were removed and post-fixed in 4% PFA
248 for 6-8 h at 4°C, and then transferred to PBS. Slices were coronal cut in a cryostat at 30 μm or in a
249 vibratome at 100 μm (Leica VT-1000, Figure 6B). Then slices were washed and mounted. Images were
250 captured using a Nikon fluorescence microscope (Nikon Ni-E) with a 10 \times objective or confocal
251 microscope (Leica SP8).

252

253 *Experimental Design and Statistical Analysis.* All sample sizes and experimental design were based on
254 previously published data from our lab and similar experiments in the field. All results were presented as
255 the mean \pm SEM. Data normality were assessed by the Kolmogorov-Smirnov test. Unpaired student's t-
256 test was used when data sets passed the normality test. The Mann-Whitney non-parametric test was used
257 for data sets not passing a normal distribution. The number of spikes and the behavioral effect of
258 chemogenetic regulation were analyzed using a two-way repeated measure ANOVA or mixed-effects
259 model. Data were analyzed and graphed using Prism 8.0 software (GraphPad, La Jolla, CA, United
260 States). The criterion for statistical significance was $P < 0.05$.

261

262 **Results**

263 **Intradermal injection of C48/80 decreases the intrinsic excitability of Drd1-MSNs in the NAc core**

264 Intradermal injection of C48/80 is a well-validated histamine-dependent itch model. As previously
265 reported (Sanders et al., 2019), injection of C48/80 caused robust scratching behaviors (Fig. 1A). In
266 addition, C48/80-treated mice show less time spent in the open arms and less number of entries into the
267 open arms on the EPM (Fig. 1B and C). The time spent in the central zone and travel distance on the OF
268 were decreased in mice treated with C48/80 (Fig. 1D and E), indicating that C48/80 induces anxiety-like
269 behaviors. We then tested whether C48/80 affects the membrane excitability of Drd1-MSNs and Drd2-
270 MSNs in the NAc core of Drd1-tdTomato and Drd2-EGFP transgenic mice using patch-clamp recordings
271 in brain slices (Fig. 1F-H). The C48/80 injection resulted in a significantly hyperpolarized RMP in Drd1-
272 MSNs (Fig. 1I) and an increased rheobase current (the minimal current necessary to elicit firing) (Fig. 1J).
273 The number of the evoked action potentials recorded from Drd1-MSNs was decreased in C48/80-treated
274 mice (Fig. 1K and L). In contrast, the RMP, rheobase current, and evoked action potentials in Drd2-
275 MSNs were comparable between saline and C48/80 groups (Fig. 1M-P).

276

277 **Chemogenetic activation of Drd1-MSNs attenuates C48/80-induced scratching behaviors**

278 Based on the alterations of intrinsic excitability in Drd1-MSNs after C48/80, we asked whether the
279 activity of Drd1-MSNs in the NAc core is involved in C48/80-induced scratching and the related anxiety.
280 The AAV expressing Cre-dependent hM3D(Gq) DREADDs (AAV-DIO-hM3Dq-mCherry) or control
281 AAVs (AAV-DIO-mCherry) were injected into the bilateral NAc core of Drd1-Cre transgenic mice (Fig.
282 2A). Mice were intraperitoneally injected with CNO or vehicle 45 min before the behaviors testing (Fig.
283 2B). The expression of AAVs in the NAc core was confirmed by mCherry fluorescence (Fig. 2C, D). The
284 *ex vivo* electrophysiological recordings showed that the excitability of Drd1-MSNs infected with AAV-
285 DIO-hM3Dq-mCherry was rapidly increased after CNO perfusion (Fig. 2E). The behavioral test showed
286 that CNO significantly suppressed C48/80-induced scratching bouts in mice injected with AAV-DIO-
287 hM3Dq-mCherry (Fig. 2F). However, in mice injected with the AAV-DIO-mCherry, CNO did not change
288 the scratching behavior. To test the effect of AAV-DIO-hM3Dq-mCherry in C48/80-induced anxiety-like
289 behavior, the EPMT and OFT were performed. For the EPMT, there was no significant difference in the
290 time spent in the open arms (Fig. 2G) and the number of entries into the open arms (Fig. 2H) between
291 vehicle and CNO treatment in AAV-DIO-hM3Dq-mCherry- or AAV-DIO-mCherry-treated mice.
292 Similarly, the activation of Drd1-MSNs had no effects on the time spent in the central zone (Fig. 2I) and
293 travel distance (Fig. 2J) on the OFT.

294

295 **Chemogenetic inhibition of Drd1-MSNs promotes a low dose of C48/80-induced scratching** 296 **behaviors**

297 We then tested the effect of chemogenetic inhibition of Drd1-MSNs on C48/80-induced behaviors. AAV
298 virus expressing Cre-dependent hM4D(Gi) DREADDs (AAV-DIO-hM4Di-mCherry) or AAV-DIO-
299 mCherry were bilaterally injected in the NAc core in Drd1-Cre transgenic mice. Mice were examined for
300 scratching and anxiety-like behaviors after CNO (or vehicle) and C48/80 injection (Fig. 3A and B). The
301 virus expression in the NAc core was confirmed by mCherry fluorescence (Fig. 3C, D). Moreover, the
302 excitability of Drd1-MSNs with AAV-DIO-hM4Di-mCherry infection was markedly decreased after
303 CNO incubation (Fig. 3E). However, inhibition of Drd1-MSNs firing by AAV-DIO-hM4Di-mCherry and

304 CNO did not affect C48/80-induced scratching behaviors (Fig. 3F). We then checked the effect of the
305 virus on itch induced by a lower dose of C48/80 (10 μ g/50 μ l). The results showed that inhibition of
306 Drd1-MSNs significantly increased scratching bouts in mice who received the lower dose of C48/80 (Fig.
307 3G). Again, inhibition of Drd1-MSNs had no effect on time spent and entries in the open arms on the
308 EPM or the time spent in the central zone and total travel distance on the OF after either common dose
309 (Fig. 3H-K) or lower dose (Fig. 3L-O) of C48/80 injection.

310

311 **Excitatory synaptic input is increased in Drd1-MSNs from C48/80-treated mice**

312 To examine if the change of neuronal excitability corresponds to the modulation of excitatory synaptic
313 inputs under itch conditions, we measured the excitatory synaptic input to Drd1- and Drd2-MSNs after
314 saline or C48/80 injection. We first tested the I-O relationships of the glutamatergic transmission
315 established by the amplitude of EPSCs versus the electrical stimulation intensity on Drd1- and Drd2-
316 MSNs. Compared to the saline-treated group, C48/80 increased the magnitude of EPSCs that were
317 evoked with the same intensity in Drd1-MSNs (Fig. 4A), but not altered in Drd2-MSNs (Fig. 4B).
318 Moreover, in Drd1-MSNs from C48/80-treated mice, there is a significant increase in the frequency of
319 sEPSCs, but not in the amplitude (Fig. 4C-E). However, C48/80 did not change the frequency or
320 amplitude of sEPSCs in Drd2-MSNs (Fig. 4 F-H). To confirm the presynaptic modulation of glutamate
321 release onto MSNs underlying itch conditions, we recorded electrical stimulation-evoked PPR on Drd1-
322 and Drd2-MSNs. Compared to the saline-treated mice, the PPR of electrical stimulus-evoked EPSCs was
323 substantially decreased in Drd1-MSNs from C48/80-treated mice (Fig. 4I). In contrast, C48/80-treated
324 mice displayed no difference from saline-treated mice in the PPR of evoked EPSCs recorded from Drd2-
325 MSNs (Fig. 4J). As it was reported that some line of Drd2-EGFP mice are hyperactive (Kramer et al.,
326 2011), we compared the locomotion activity of Drd2-EGFP mice with C57Bl/6 mice. It showed that the
327 travel distance is comparable between the two groups (Drd2-EGFP vs. C57Bl/6, 15.5 ± 1.4 m vs. $16.3 \pm$

328 1.7 m. $P = 0.5699$, Mann-Whitney test, $n = 8-14$ mice/group), which is in agreement with the reports by
329 Chan et al.(Chan et al., 2012), indicating that the data from our Drd2-EGFP mice are reliable.

330

331 **C48/80 induces pathway-specific changes of glutamatergic synaptic input onto Drd1-MSNs**

332 The NAc receives glutamate synaptic input from the mPFC, BLA, and vHipp (Friedman et al., 2002; Britt
333 et al., 2012). To test which pathway contributes to acute itch-induced presynaptic alterations, we injected
334 AAV expressing YFP-tagged channel rhodopsin 2 (AAV9-CaMKII α -ChR2-eYFP) into the mPFC, BLA,
335 or vHipp. Three to four weeks later, notable expression of ChR2 was shown within these regions, and
336 fluorescent axons were concentrated in NAc core (Fig. 5A). Then we validated the ChR2 function in
337 YFP-positive pyramidal neurons in the mPFC and the afferents onto Drd1-MSNs in the NAc. The light-
338 stimulation (470 nm, 2-5 mW, with 5 Hz, 10 Hz, and 20 Hz for 1 sec) evoked stable firing in pyramidal
339 neurons in the mPFC (Fig. 5B). Moreover, the light-stimulation-evoked EPSCs in Drd1-MSNs were
340 blocked by adding DNQX (20 μ M), an antagonist of AMPA/kainate receptor (Fig. 5C). Then we tested
341 the presynaptic efficacies at afferents from mPFC, BLA, or vHipp onto Drd1-MSN in individual groups
342 of animals using PPR. In Drd1-MSNs of the NAc core from C48/80-treated animals, the PPR of light-
343 evoked EPSC at mPFC afferent synapses was significantly decreased, but no change of PPR in BLA- or
344 vHipp-NAc synaptic afferents (Fig. 5D and E). To clarify whether C48/80 changes the postsynaptic
345 glutamate receptor's function at these afferents onto Drd1-MSNs, we measured the light-evoked currents
346 mediated by AMPA and NMDA receptors. However, there was no difference in AMPAR/NMDAR
347 response ratios in mPFC-, BLA-, or vHipp-NAc synapses between saline and C48/80 injection groups
348 (Fig. 5F). These results suggest that C48/80 induces a presynaptic adaptive change in mPFC-NAc
349 projections onto Drd1-MSNs in the NAc core.

350

351 **The intrinsic excitability of mPFC-NAc projecting neurons is increased in C48/80-injected mice**

352 To test whether C48/80-induced change of transmitter release corresponds to the activity of the upstream
353 region mPFC, the membrane excitability of mPFC-NAc projecting pyramidal neurons was assessed in

354 mice with NAc injection of retrobeads. Seven days after NAc injection, the retrobeads-positive pyramidal
355 neurons were observed in the mPFC (Fig. 6A and B). We recorded the membrane physiological
356 properties on labeled mPFC-NAc projecting pyramidal neurons in layer V of the PFC slice (Fig. 6C).
357 C48/80 did not change the RMP in the mPFC-NAc projecting neurons (Fig. 6D), while significantly
358 decreased rheobase currents (Fig. 6E). Additionally, the current-induced neuronal firing in mPFC-NAc
359 projecting neurons was significantly increased in C48/80-injected mice (Fig. 6F and G).

360

361 **Chemogenetic suppression of mPFC-NAc excitatory synaptic afferents relieves C48/80-induced itch**
362 **behavior**

363 We then measured whether the changes in the activity of mPFC-NAc excitatory synaptic input are related
364 to itching behaviors. To examine this, AAV virus encoding inhibitory hM4D(Gi) DREADDs (AAV-
365 CaMKII α -hM4Di-mCherry) or AAV-CaMKII α -mCherry were bilaterally injected into the mPFC with
366 bilateral implantation the guided cannulas into the NAc core (Fig. 7A). Mice were examined for
367 scratching and anxiety-like behaviors after intradermal injection of C48/80 and intra-NAc local infusion
368 of either vehicle or CNO before testing (Fig. 7B). The AAV injection site in the mPFC and the axon
369 terminal expression in the NAc core were verified by mCherry fluorescence (Fig. 7C, D). The behavioral
370 results showed that the CNO infusion into the NAc core significantly suppressed the scratching bouts in
371 mice expressing the AAV-CaMKII α -hM4Di-mCherry but not in mice expressing AAV-CaMKII α -
372 mCherry after C48/80 injection (Fig. 7E). Furthermore, chemogenetic inhibition of mPFC-NAc core
373 synaptic pathway had no effect on the time spent in the open arms (Fig. 7F) and number of entries into the
374 open arms (Fig. 7G) on the EPM or the time spent in central zone (Fig. 7H) and travel distance (Fig. 7I)
375 on the OF.

376

377 **Pharmacological regulation of KOR in the NAc alters C48/80-induced scratching behaviors**

378 Activation of KOR has been adopted to treat intractable itch (Wikstrom et al., 2005; Munanairi et al.,
379 2018). Moreover, human functional magnetic resonance imaging showed that the NAc mediates the

380 antipruritic effect of KOR activation (Papoiu et al., 2015). To examine the role of KOR in itch processing,
381 the bilateral guide cannulas were implanted into the NAc core. After the surgery recovery, KOR agonist
382 U50488 was infused into the NAc core and the behaviors were tested (Fig. 8A and B). U50488
383 significantly decreased the scratching behavior induced by C48/80 (Fig. 8C). There were no effect on the
384 time spent (Fig. 8D) and entries (Fig. 8E) in the open arms on the EPM, or the time spent in the central
385 zone (Fig. 8F) and total travel distance (Fig. 8G) on the OF after activation of KOR. In contrast, low dose
386 of C48/80-induced scratching behaviors were significantly increased after the infusion of a KOR
387 antagonist nor-NBI into the NAc core (Fig. 8H). On the EPM, there was no significant difference between
388 vehicle- and nor-NBI-treated mice in time spent in the open arms (Fig. 8I) and the number of entries into
389 the open arms (Fig. 8J). Similarly, nor-NBI infusion had no effects on the time spent in the central zone
390 (Fig. 8K) and travel distance (Fig. 8L) on the OF in C48/80-treated animals.

391

392 **The activity of KOR regulates itch-related synaptic plasticity in the NAc core**

393 To further test the mechanisms underlying KOR-mediated modulation of scratching behavior induced by
394 C48/80, we recorded mEPSCs in the Drd1-MSNs from saline- and C48/80-injected mice. We first
395 measured the effects of U50488 on mEPSCs of Drd1-MSNs (Fig. 9A). Perfusion of U50488 significantly
396 decreased the frequency of mEPSCs in Drd1-MSN recorded from C48/80-treated animals compared with
397 that in saline-treated mice (Fig. 9B). No difference was observed on the amplitude of mEPSCs in saline-
398 and C48/80-treated mice (Fig. 9C). Moreover, inhibition of KOR with nor-NBI increased the frequency
399 of mEPSCs in Drd1-MSNs from C48/80-treated mice (Fig. 9D, E), with no alterations in the amplitude of
400 mEPSCs (Fig. 9D, F).

401

402 **Discussion**

403 Here we showed that C48/80 decreased the intrinsic membrane excitability in Drd1-MSNs, and
404 chemogenetic activation of Drd1-MSNs attenuated C48/80-induced itch. Moreover, C48/80 increased the
405 excitatory synaptic transmission of Drd1-MSNs from the mPFC, also increased the intrinsic excitability

406 of PFC-NAc projecting pyramidal neurons. Chemogenetic inhibition of the PFC-NAc synaptic pathway
407 relieved C48/80-induced scratching. Furthermore, pharmacological activation of KOR in the NAc
408 suppressed scratching behavior and reduced the presynaptic excitatory inputs to Drd1-MSNs. Our results
409 suggest that Drd1-MSNs and the synaptic inputs from the mPFC play an important role in the regulation
410 of the scratching behaviors induced by itch stimuli, and KOR acts as a negative feedback regulator of
411 Drd1-MSNs at the NAc core under itch conditions.

412

413 **Neural adaptation of Drd1-MSNs in the NAc core in C48/80-elicited acute itch**

414 As a critical part of the reward circuit, the NAc MSNs receive dopaminergic innervation from the VTA
415 (Stuber et al., 2011). Meanwhile, NAc sends long-range GABAergic synaptic axonal projections to the
416 VTA (Watabe-Uchida et al., 2012; Yang et al., 2018), and these inhibitory inputs play a major role in
417 controlling the activity of DA neurons (Henny et al., 2012). C48/80 decreased the intrinsic excitability of
418 Drd1-MSNs in the NAc, which may reduce the inhibition on VTA DA neurons and increase the release of
419 DA to the NAc. Indeed, the activity of VTA DA neurons was increased during scratching behavior (Yuan
420 et al., 2018; Su et al., 2019), and repeated activation of dopamine receptors on NAc neurons caused a
421 reduction of membrane excitability (O'Donnell and Grace, 1996). Meanwhile, Drd1-MSNs suppress the
422 tonic activity of VTA GABA neurons (Bocklisch et al., 2013), and the decreased intrinsic excitability of
423 Drd1-MSNs may also contribute to the increased activity of GABA neurons under acute itch conditions,
424 which mediates itch-related aversion (Su et al., 2019). Our data also showed that the RMP was
425 hyperpolarized in Drd1-MSNs, which may also contribute to the decreased neuronal excitability after itch
426 stimuli. However, the intrinsic excitability of Drd2-MSNs was not changed after C48/80 injection,
427 indicating a different role of these two subtypes in mediating itch.

428 The Drd1-MSNs play a crucial role in regulating the desire and motivation in reward-related
429 behaviors (Calipari et al., 2016). Moreover, activation of NAc Drd1-MSNs results in resilient behavioral
430 outcomes, while inhibition of these MSNs induces depression-like outcomes after chronic social defeat

431 stress (CSDC) (Francis et al., 2015). Chemogenetic activation of Drd1-MSNs decreased the scratching
432 behaviors, which may be due to the increased GABAergic inhibition on dopaminergic neurons in the
433 VTA (Yang et al., 2018). Meanwhile, chemogenetic inhibition of Drd1-MSNs enhanced scratching bouts
434 in the low dose of C48/80 exposure but did not in the normal dose of C48/80 injection, which may
435 attribute to the relative ceiling effect of C48/80 on scratching production (Kuraishi et al., 1995). However,
436 chemogenetic regulation of the activity of NAc Drd1-MSNs had no effect on itch-elicited anxiety-like
437 behaviors, suggesting that the motivation to scratch may be separated from the anxiety-like behaviors.

438 NAc MSNs are a special type of GABAergic inhibitory neurons without spontaneous action
439 potentials discharge, causing its activity depend on synaptic afferents. Itch stimuli increased the frequency
440 but not the amplitude of sEPSCs in Drd1-MSNs, suggesting a presynaptic change in Drd1-MSNs, which
441 was confirmed by measuring the electrical stimuli-evoked EPSC PPR, further suggesting that the
442 adaption of presynaptic mechanism may increase the I-O relationship of EPSCs in Drd1-MSNs under itch
443 conditions. The itch-elicited scratching behavior is highly associated with an increase in NAc DA level
444 (Yuan et al., 2018), and DA or Drd1 agonist increased sEPSC frequency in Drd1-MSNs, while Drd2
445 agonist decreased sEPSCs frequency in Drd2-MSNs (Andre et al., 2010). Meanwhile, the excitatory
446 transmission was decreased in NAc Drd2-MSNs in inflammatory pain model (Schwartz et al., 2014).
447 Notably, the increased presynaptic transmission is associated with the decreased membrane excitability of
448 Drd1-MSNs after C48/80 injection, suggesting a synapse-membrane homeostatic regulation under acute
449 itch conditions. An increase in the excitatory synaptic strength causes a homeostatic decrease in the
450 intrinsic membrane excitability of NAc MSNs, which tends to stabilize the functional output of neuron
451 (Ishikawa et al., 2009; Wang et al., 2018). It was reported that the upregulation of glutamate receptor
452 NR2B leads to a decrease in the membrane excitability of NAc MSNs after short-term cocaine
453 withdrawal (Wang et al., 2018). The molecular mechanism underlying the decrease of the membrane
454 excitability of Drd1-MSNs after C48/80 needs further investigation.

455

456 **mPFC-NAc projections are adaptively changed and implicated in itch-related scratching**

457 Glutamatergic synaptic afferents from multiple limbic and paralimbic regions to the NAc MSNs
458 contribute to the regulation of motivation and anxiety (Stuber et al., 2011; Calhoun and Tye, 2015; Zhang
459 et al., 2020). C48/80 did not change the AMPAR/NMDAR current ratio from mPFC, vHipp, and BLA,
460 suggesting that the postsynaptic mechanism is not involved in acute itch. Similarly, cocaine exposure
461 selectively increases the presynaptic release probability of the PFC-NAc synapses but does not change the
462 BLA-NAc synapses (Suska et al., 2013). Differently, nerve injury- or inflammation-induced chronic pain
463 causes long-term changes in postsynaptic AMPAR and NMDARs, and a decrease in the related
464 motivation (Ren et al., 2016).

465 Some cortex regions including mPFC, ACC, and insular cortex are activated under itch conditions
466 (Dhand and Aminoff, 2014; Chen and Sun, 2020). C48/80 increased the intrinsic excitability of PFC-NAc
467 projecting pyramidal neurons, which corresponds to the increase of glutamate release at the presynaptic
468 terminals of these projection neurons in the NAc since the frequency of the action potential is closely
469 related to glutamate transmitter release (Kaczmarek and Zhang, 2017). In agreement with the current
470 study, c-fos expression was increased in the mPFC and ACC regions but not in BLA in mice with
471 histamine-induced acute itch (Lu et al., 2018). Chemogenetic inhibition of PFC reduced both
472 histaminergic and non-histaminergic itch-induced scratching (Li et al., 2021). Here, selective inhibition of
473 the mPFC-NAc projection reduced C48/80-induced scratching behaviors. However, it seems
474 contradictory to the increased scratching after the inhibition of Drd1-MSNs, which may be due to the
475 complicated local circuitry in the NAc. Drd1-MSNs receive not only excitatory inputs from pPFC, vHipp,
476 and BLA and DAergic input from VTA, but also inhibitory inputs from local GABAergic Drd2-MSNs,
477 cholinergic and fast-spiking GABAergic interneurons (Stuber et al., 2012). The inhibition of mPFC-NAc
478 projection or activation of KOR may lead to the changes of other pathways and indirectly regulate the
479 excitability of Drd1-MSNs.

480 Optogenetic regulation of mPFC or mPFC-NAc axonal terminals changes pain-related negative
481 emotions (Lee et al., 2015; Martinez et al., 2017; Zhou et al., 2018). However, inhibition of the mPFC-
482 NAc pathway did not change itch-related anxiety behaviors. It was reported that selective stimulation of

483 the mPFC-NAc pathway did not change anxiety-like behavior on OFT, but inhibition of the vHipp-NAc
484 pathway improves the depressive emotion in the CSDS model (Bagot et al., 2015), supporting that
485 pathway-specific regulation of excitatory afferent onto the NAc displays disparate behavioral and
486 physiological responses (Stuber et al., 2012). The neural circuits for coding the anxiety-like behaviors in
487 itch require further experiments.

488

489 **KOR activation regulates acute itch via a presynaptic mechanism in the NAc core**

490 Human studies showed that injection with butorphanol, a pronounced KOR affinity agonist, suppresses
491 histamine-evoked itch via the activation of NAc and septal nuclei (Papoiu et al., 2015). Systemic
492 activation of KOR prevents the scratching behaviors induced by chloroquine in male mice (Brust et al.,
493 2016). Consistently, we found that activation of KOR in the NAc core attenuated C48/80-elicited
494 scratching. KOR is expressed on presynaptic terminals of glutamate, dopamine, and serotonin inputs to
495 the NAc (Karkhanis et al., 2016; Rose et al., 2016; Fontaine et al., 2022). Dynorphin is known to be the
496 endogenous ligand of KOR, which is predominantly expressed in Drd1-MSNs in the NAc. The decrease
497 of excitability of Drd1-MSNs after C48/80 may cause a reduction of dynorphin release. The activation of
498 KORs inhibited excitatory synaptic transmission on Drd1-MSNs in itch animals, which may be due to
499 negative feedback inhibition of KOR on the excitatory synaptic inputs from the mPFC (Hjelmstad and
500 Fields, 2001). Glutamatergic afferents into Drd1-MSNs but not into Drd2-MSNs are more sensitive to
501 KOR inhibition, and KOR inhibits BLA-NAc excitatory synaptic transmission in Drd1-MSNs (Tejeda et
502 al., 2017). Moreover, activation of KOR in the caudal NAc shell or rostral NAc shell increased or
503 decreased anxiety-like behaviors, respectively (Pirino et al., 2020). We found that C48/80-induced
504 anxiety-like behaviors were not changed by KOR ligand in the NAc core, indicating that KOR modulates
505 itch-related behaviors potentially via a cell-type and neural circuit-specific manner.

506 In summary, our study elucidated the role of NAc MSN subtypes and their glutamatergic excitatory
507 afferents in itch-related behaviors. These results demonstrated that the synaptic connections from mPFC
508 to NAc core shaped the itch stimuli-elicited scratching behavior. In addition, NAc KOR acts as a negative

509 feedback regulator to drive itch-elicited scratching. Thus, specific regulation of the projection from mPFC
510 to Drd1-MSNs or regulation of KOR in NAc core may provide effective strategies for the treatment of
511 itch. It is worth noting that the current study was performed in male mice, whether the mechanisms work
512 in female mice need further investigation.

513

514 **Author contributions**

515 X.-B. Wu and Y.-J. Gao designed the research. Q. Zhu, M.-H. Gao, S.-X. Yan, P.-Y. Gu, P.-F. Zhang,
516 and M.-L. Xu performed research; Q. Zhu, M.-H. Gao, and S.-X. Yan analyzed data; X.-B. Wu wrote the
517 draft of the paper; Y.-J. Gao edited the paper.

518

519 **References**

- 520 Andre VM, Cepeda C, Cummings DM, Jocoy EL, Fisher YE, William Yang X, Levine MS (2010) Dopamine
521 modulation of excitatory currents in the striatum is dictated by the expression of D1 or D2
522 receptors and modified by endocannabinoids. *Eur J Neurosci* 31:14-28.
- 523 Bagot RC, Parise EM, Pena CJ, Zhang HX, Maze I, Chaudhury D, Persaud B, Cachope R, Bolanos-Guzman
524 CA, Cheer JF, Deisseroth K, Han MH, Nestler EJ (2015) Ventral hippocampal afferents to the
525 nucleus accumbens regulate susceptibility to depression. *Nat Commun* 6:7062.
- 526 Bartels DJ, van Laarhoven AI, van de Kerkhof PC, Evers AW (2016) Placebo and nocebo effects on itch:
527 effects, mechanisms, and predictors. *Eur J Pain* 20:8-13.
- 528 Bocklisch C, Pascoli V, Wong JC, House DR, Yvon C, de Roo M, Tan KR, Luscher C (2013) Cocaine
529 disinhibits dopamine neurons by potentiation of GABA transmission in the ventral tegmental
530 area. *Science* 341:1521-1525.
- 531 Britt JP, Benaliouad F, McDevitt RA, Stuber GD, Wise RA, Bonci A (2012) Synaptic and behavioral profile
532 of multiple glutamatergic inputs to the nucleus accumbens. *Neuron* 76:790-803.
- 533 Brust TF, Morgenweck J, Kim SA, Rose JH, Locke JL, Schmid CL, Zhou L, Stahl EL, Cameron MD, Scarry SM,
534 Aube J, Jones SR, Martin TJ, Bohn LM (2016) Biased agonists of the kappa opioid receptor
535 suppress pain and itch without causing sedation or dysphoria. *Sci Signal* 9:ra117.
- 536 Calhoun GG, Tye KM (2015) Resolving the neural circuits of anxiety. *Nat Neurosci* 18:1394-1404.
- 537 Calipari ES, Bagot RC, Purushothaman I, Davidson TJ, Yorgason JT, Pena CJ, Walker DM, Pirpinias ST,
538 Guise KG, Ramakrishnan C, Deisseroth K, Nestler EJ (2016) In vivo imaging identifies temporal
539 signature of D1 and D2 medium spiny neurons in cocaine reward. *Proc Natl Acad Sci U S A*
540 113:2726-2731.
- 541 Chan CS, Peterson JD, Gertler TS, Glajch KE, Quintana RE, Cui Q, Sebel LE, Plotkin JL, Shen W, Heiman M,
542 Heintz N, Greengard P, Surmeier DJ (2012) Strain-specific regulation of striatal phenotype in
543 Drd2-eGFP BAC transgenic mice. *J Neurosci* 32:9124-9132.
- 544 Chartoff EH, Ebner SR, Sparrow A, Potter D, Baker PM, Ragozzino ME, Roitman MF (2016) Relative
545 Timing Between Kappa Opioid Receptor Activation and Cocaine Determines the Impact on
546 Reward and Dopamine Release. *Neuropsychopharmacology* 41:989-1002.

-
- 547 Chen XJ, Sun YG (2020) Central circuit mechanisms of itch. *Nat Commun* 11:3052.
- 548 Chisholm A, Rizzo D, Fortin E, Moman V, Quteishat N, Romano A, Capolicchio T, Shalev U (2021)
- 549 Assessing the Role of Corticothalamic and Thalamo-Accumbens Projections in the Augmentation
- 550 of Heroin Seeking in Chronically Food-Restricted Rats. *J Neurosci* 41:354-365.
- 551 Dhand A, Aminoff MJ (2014) The neurology of itch. *Brain* 137:313-322.
- 552 Floresco SB (2015) The nucleus accumbens: an interface between cognition, emotion, and action. *Annu*
- 553 *Rev Psychol* 66:25-52.
- 554 Fontaine HM, Silva PR, Neiswanger C, Tran R, Abraham AD, Land BB, Neumaier JF, Chavkin C (2022)
- 555 Stress decreases serotonin tone in the nucleus accumbens in male mice to promote aversion
- 556 and potentiate cocaine preference via decreased stimulation of 5-HT1B receptors.
- 557 *Neuropsychopharmacology* 47:891-901.
- 558 Francis TC, Chandra R, Friend DM, Finkel E, Dayrit G, Miranda J, Brooks JM, Iniguez SD, O'Donnell P,
- 559 Kravitz A, Lobo MK (2015) Nucleus accumbens medium spiny neuron subtypes mediate
- 560 depression-related outcomes to social defeat stress. *Biol Psychiatry* 77:212-222.
- 561 Friedman DP, Aggleton JP, Saunders RC (2002) Comparison of hippocampal, amygdala, and perirhinal
- 562 projections to the nucleus accumbens: combined anterograde and retrograde tracing study in
- 563 the Macaque brain. *J Comp Neurol* 450:345-365.
- 564 Henny P, Brown MT, Northrop A, Faunes M, Ungless MA, Magill PJ, Bolam JP (2012) Structural correlates
- 565 of heterogeneous in vivo activity of midbrain dopaminergic neurons. *Nat Neurosci* 15:613-619.
- 566 Hjelmstad GO, Fields HL (2001) Kappa opioid receptor inhibition of glutamatergic transmission in the
- 567 nucleus accumbens shell. *J Neurophysiol* 85:1153-1158.
- 568 Ishikawa M, Mu P, Moyer JT, Wolf JA, Quock RM, Davies NM, Hu XT, Schluter OM, Dong Y (2009)
- 569 Homeostatic synapse-driven membrane plasticity in nucleus accumbens neurons. *J Neurosci*
- 570 29:5820-5831.
- 571 Jing PB, Cao DL, Li SS, Zhu M, Bai XQ, Wu XB, Gao YJ (2018) Chemokine Receptor CXCR3 in the Spinal
- 572 Cord Contributes to Chronic Itch in Mice. *Neurosci Bull* 34:54-63.
- 573 Kaczmarek LK, Zhang Y (2017) Kv3 Channels: Enablers of Rapid Firing, Neurotransmitter Release, and
- 574 Neuronal Endurance. *Physiol Rev* 97:1431-1468.
- 575 Kallupi M, Wee S, Edwards S, Whitfield TW, Jr., Oleata CS, Luu G, Schmeichel BE, Koob GF, Roberto M
- 576 (2013) Kappa opioid receptor-mediated dysregulation of gamma-aminobutyric acidergic
- 577 transmission in the central amygdala in cocaine addiction. *Biol Psychiatry* 74:520-528.
- 578 Karkhanis AN, Rose JH, Weiner JL, Jones SR (2016) Early-Life Social Isolation Stress Increases Kappa
- 579 Opioid Receptor Responsiveness and Downregulates the Dopamine System.
- 580 *Neuropsychopharmacology* 41:2263-2274.
- 581 Kramer PF, Christensen CH, Hazelwood LA, Dobi A, Bock R, Sibley DR, Mateo Y, Alvarez VA (2011)
- 582 Dopamine D2 receptor overexpression alters behavior and physiology in *Drd2-EGFP* mice. *J*
- 583 *Neurosci* 31:126-132.
- 584 Kreitzer AC (2009) Physiology and pharmacology of striatal neurons. *Annu Rev Neurosci* 32:127-147.
- 585 Kuraishi Y, Nagasawa T, Hayashi K, Satoh M (1995) Scratching behavior induced by pruritogenic but not
- 586 algesciogenic agents in mice. *Eur J Pharmacol* 275:229-233.
- 587 Lavery MJ, Stull C, Kinney MO, Yosipovitch G (2016) Nocturnal Pruritus: The Battle for a Peaceful Night's
- 588 Sleep. *Int J Mol Sci* 17:425.
- 589 Lee M, Manders TR, Eberle SE, Su C, D'Amour J, Yang R, Lin HY, Deisseroth K, Froemke RC, Wang J (2015)
- 590 Activation of corticostriatal circuitry relieves chronic neuropathic pain. *J Neurosci* 35:5247-5259.
- 591 LeGates TA, Kvarita MD, Tooley JR, Francis TC, Lobo MK, Creed MC, Thompson SM (2018) Reward
- 592 behaviour is regulated by the strength of hippocampus-nucleus accumbens synapses. *Nature*
- 593 564:258-262.

- 594 Li X, Yao J, Hu KH, Wu B, Sui JF, Gao J, Wu GY, Liu SL (2021) Differential roles of prelimbic and anterior
595 cingulate cortical region in the modulation of histaminergic and non-histaminergic itch. *Behav*
596 *Brain Res* 411:113388.
- 597 Lu YC, Wang YJ, Lu B, Chen M, Zheng P, Liu JG (2018) ACC to Dorsal Medial Striatum Inputs Modulate
598 Histaminergic Itch Sensation. *J Neurosci* 38:3823-3839.
- 599 Martinez E, Lin HH, Zhou H, Dale J, Liu K, Wang J (2017) Corticostriatal Regulation of Acute Pain. *Front*
600 *Cell Neurosci* 11:146.
- 601 Massaly N, Copits BA, Wilson-Poe AR, Hipolito L, Markovic T, Yoon HJ, Liu S, Walicki MC, Bhatti DL, Sirohi
602 S, Klaas A, Walker BM, Neve R, Cahill CM, Shoghi KI, Gereau RWt, McCall JG, Al-Hasani R,
603 Bruchas MR, Moron JA (2019) Pain-Induced Negative Affect Is Mediated via Recruitment of The
604 Nucleus Accumbens Kappa Opioid System. *Neuron* 102:564-573 e566.
- 605 Mochizuki H, Tanaka S, Morita T, Wasaka T, Sadato N, Kakigi R (2014) The cerebral representation of
606 scratching-induced pleasantness. *J Neurophysiol* 111:488-498.
- 607 Mochizuki H, Papoiu ADP, Nattkemper LA, Lin AC, Kraft RA, Coghill RC, Yosipovitch G (2015) Scratching
608 Induces Overactivity in Motor-Related Regions and Reward System in Chronic Itch Patients. *J*
609 *Invest Dermatol* 135:2814-2823.
- 610 Mu P, Neumann PA, Panksepp J, Schluter OM, Dong Y (2011) Exposure to cocaine alters dynorphin-
611 mediated regulation of excitatory synaptic transmission in nucleus accumbens neurons. *Biol*
612 *Psychiatry* 69:228-235.
- 613 Munanairi A et al. (2018) Non-canonical Opioid Signaling Inhibits Itch Transmission in the Spinal Cord of
614 Mice. *Cell Rep* 23:866-877.
- 615 Murota H, Kitaba S, Tani M, Wataya-Kaneda M, Azukizawa H, Tanemura A, Umegaki N, Terao M,
616 Kotobuki Y, Katayama I (2010) Impact of sedative and non-sedative antihistamines on the
617 impaired productivity and quality of life in patients with pruritic skin diseases. *Allergol Int*
618 59:345-354.
- 619 O'Donnell P, Grace AA (1996) Dopaminergic reduction of excitability in nucleus accumbens neurons
620 recorded in vitro. *Neuropsychopharmacology* 15:87-97.
- 621 Papoiu AD, Nattkemper LA, Sanders KM, Kraft RA, Chan YH, Coghill RC, Yosipovitch G (2013) Brain's
622 reward circuits mediate itch relief. a functional MRI study of active scratching. *PLoS One*
623 8:e82389.
- 624 Papoiu ADP, Kraft RA, Coghill RC, Yosipovitch G (2015) Butorphanol suppression of histamine itch is
625 mediated by nucleus accumbens and septal nuclei: a pharmacological fMRI study. *J Invest*
626 *Dermatol* 135:560-568.
- 627 Phan NQ, Lotts T, Antal A, Bernhard JD, Stander S (2012) Systemic kappa opioid receptor agonists in the
628 treatment of chronic pruritus: a literature review. *Acta Derm Venereol* 92:555-560.
- 629 Pirino BE, Spodnick MB, Gargiulo AT, Curtis GR, Barson JR, Karkhanis AN (2020) Kappa-opioid receptor-
630 dependent changes in dopamine and anxiety-like or approach-avoidance behavior occur
631 differentially across the nucleus accumbens shell rostral-caudal axis. *Neuropharmacology*
632 181:108341.
- 633 Ren W, Centeno MV, Berger S, Wu Y, Na X, Liu X, Kondapalli J, Apkarian AV, Martina M, Surmeier DJ
634 (2016) The indirect pathway of the nucleus accumbens shell amplifies neuropathic pain. *Nat*
635 *Neurosci* 19:220-222.
- 636 Rose JH, Karkhanis AN, Chen R, Gioia D, Lopez MF, Becker HC, McCool BA, Jones SR (2016)
637 Supersensitive Kappa Opioid Receptors Promotes Ethanol Withdrawal-Related Behaviors and
638 Reduce Dopamine Signaling in the Nucleus Accumbens. *Int J Neuropsychopharmacol* 19.
- 639 Samineni VK, Grajales-Reyes JG, Grajales-Reyes GE, Tycksen E, Copits BA, Pedersen C, Ankudey ES,
640 Sackey JN, Sewell SB, Bruchas MR, Gereau RW (2021) Cellular, circuit and transcriptional
641 framework for modulation of itch in the central amygdala. *Elife* 10.

-
- 642 Sanders KM, Akiyama T (2018) The vicious cycle of itch and anxiety. *Neurosci Biobehav Rev* 87:17-26.
- 643 Sanders KM, Sakai K, Henry TD, Hashimoto T, Akiyama T (2019) A Subpopulation of Amygdala Neurons
- 644 Mediates the Affective Component of Itch. *J Neurosci* 39:3345-3356.
- 645 Schwartz N, Temkin P, Jurado S, Lim BK, Heifets BD, Polepalli JS, Malenka RC (2014) Chronic pain.
- 646 Decreased motivation during chronic pain requires long-term depression in the nucleus
- 647 accumbens. *Science* 345:535-542.
- 648 Soares-Cunha C, Coimbra B, Sousa N, Rodrigues AJ (2016) Reappraising striatal D1- and D2-neurons in
- 649 reward and aversion. *Neurosci Biobehav Rev* 68:370-386.
- 650 Stuber GD, Britt JP, Bonci A (2012) Optogenetic modulation of neural circuits that underlie reward
- 651 seeking. *Biol Psychiatry* 71:1061-1067.
- 652 Stuber GD, Sparta DR, Stamatakis AM, van Leeuwen WA, Hardjoprajitno JE, Cho S, Tye KM, Kempadoo
- 653 KA, Zhang F, Deisseroth K, Bonci A (2011) Excitatory transmission from the amygdala to nucleus
- 654 accumbens facilitates reward seeking. *Nature* 475:377-380.
- 655 Su XY, Chen M, Yuan Y, Li Y, Guo SS, Luo HQ, Huang C, Sun W, Li Y, Zhu MX, Liu MG, Hu J, Xu TL (2019)
- 656 Central Processing of Itch in the Midbrain Reward Center. *Neuron* 102:858-872 e855.
- 657 Suska A, Lee BR, Huang YH, Dong Y, Schluter OM (2013) Selective presynaptic enhancement of the
- 658 prefrontal cortex to nucleus accumbens pathway by cocaine. *Proc Natl Acad Sci U S A* 110:713-
- 659 718.
- 660 Tejada HA, Wu J, Kornspun AR, Pignatelli M, Kashtelyan V, Krashes MJ, Lowell BB, Carlezon WA, Jr.,
- 661 Bonci A (2017) Pathway- and Cell-Specific Kappa-Opioid Receptor Modulation of Excitation-
- 662 Inhibition Balance Differentially Gates D1 and D2 Accumbens Neuron Activity. *Neuron* 93:147-
- 663 163.
- 664 Wang J, Ishikawa M, Yang Y, Otaka M, Kim JY, Gardner GR, Stefanik MT, Milovanovic M, Huang YH, Hell
- 665 JW, Wolf ME, Schluter OM, Dong Y (2018) Cascades of Homeostatic Dysregulation Promote
- 666 Incubation of Cocaine Craving. *J Neurosci* 38:4316-4328.
- 667 Wang Y, Liu Z, Cai L, Guo R, Dong Y, Huang YH (2020) A Critical Role of Basolateral Amygdala-to-Nucleus
- 668 Accumbens Projection in Sleep Regulation of Reward Seeking. *Biol Psychiatry* 87:954-966.
- 669 Watabe-Uchida M, Zhu L, Ogawa SK, Vamanrao A, Uchida N (2012) Whole-brain mapping of direct
- 670 inputs to midbrain dopamine neurons. *Neuron* 74:858-873.
- 671 Wikstrom B, Gellert R, Ladefoged SD, Danda Y, Akai M, Ide K, Ogasawara M, Kawashima Y, Ueno K, Mori
- 672 A, Ueno Y (2005) Kappa-opioid system in uremic pruritus: multicenter, randomized, double-blind,
- 673 placebo-controlled clinical studies. *J Am Soc Nephrol* 16:3742-3747.
- 674 Wu XB, Jing PB, Zhang ZJ, Cao DL, Gao MH, Jiang BC, Gao YJ (2018) Chemokine receptor CCR2
- 675 contributes to neuropathic pain and the associated depression via increasing NR2B-mediated
- 676 currents in both D1 and D2 dopamine receptor-containing medium spiny neurons in the nucleus
- 677 accumbens shell. *Neuropsychopharmacology* 43:2320-2330.
- 678 Wu ZH, Shao HY, Fu YY, Wu XB, Cao DL, Yan SX, Sha WL, Gao YJ, Zhang ZJ (2021) Descending Modulation
- 679 of Spinal Itch Transmission by Primary Somatosensory Cortex. *Neurosci Bull* 37:1345-1350.
- 680 Yang H, de Jong JW, Tak Y, Peck J, Bateup HS, Lammel S (2018) Nucleus Accumbens Subnuclei Regulate
- 681 Motivated Behavior via Direct Inhibition and Disinhibition of VTA Dopamine Subpopulations.
- 682 *Neuron* 97:434-449 e434.
- 683 Yuan L, Dou YN, Sun YG (2019) Topography of Reward and Aversion Encoding in the Mesolimbic
- 684 Dopaminergic System. *J Neurosci* 39:6472-6481.
- 685 Yuan L, Liang TY, Deng J, Sun YG (2018) Dynamics and Functional Role of Dopaminergic Neurons in the
- 686 Ventral Tegmental Area during Itch Processing. *J Neurosci* 38:9856-9869.
- 687 Zachariae R, Lei U, Haedersdal M, Zachariae C (2012) Itch severity and quality of life in patients with
- 688 pruritus: preliminary validity of a Danish adaptation of the itch severity scale. *Acta Derm*
- 689 *Venerol* 92:508-514.

-
- 690 Zahm DS, Brog JS (1992) On the significance of subterritories in the "accumbens" part of the rat ventral
691 striatum. *Neuroscience* 50:751-767.
- 692 Zhang TT, Guo SS, Wang HY, Jing Q, Yi X, Hu ZH, Yu XR, Xu TL, Liu MG, Zhao X (2022) An Anterior
693 Cingulate Cortex-to-Midbrain Projection Controls Chronic Itch in Mice. *Neurosci Bull.*
- 694 Zhang XY, Peng SY, Shen LP, Zhuang QX, Li B, Xie ST, Li QX, Shi MR, Ma TY, Zhang Q, Wang JJ, Zhu JN
695 (2020) Targeting presynaptic H3 heteroreceptor in nucleus accumbens to improve anxiety and
696 obsessive-compulsive-like behaviors. *Proc Natl Acad Sci U S A* 117:32155-32164.
- 697 Zhou H, Martinez E, Lin HH, Yang R, Dale JA, Liu K, Huang D, Wang J (2018) Inhibition of the Prefrontal
698 Projection to the Nucleus Accumbens Enhances Pain Sensitivity and Affect. *Front Cell Neurosci*
699 12:240.
- 700
- 701
- 702
- 703
- 704
- 705
- 706
- 707
- 708
- 709
- 710
- 711
- 712
- 713
- 714
- 715
- 716
- 717
- 718
- 719

720 **Figures legend**

721 **Figure 1. C48/80 reduces intrinsic excitability of Drd1-MSNs in the NAc core.** **A**, Intradermal
722 injection of C48/80 induces scratching bouts in mice. (n = 13-14 mice/group, *** $P < 0.0001$, $U = 0$,
723 Mann–Whitney U test). **B**, The EPMT shows that C48/80 treatment reduces the time spent in open arms
724 compared with saline injection (n = 13-14 mice/group, ** $P = 0.0069$, $U = 36.50$, Mann–Whitney U test).
725 **C**, C48/80 reduces the open arms entries on the EPM (*** $P < 0.0001$, $t_{25} = 4.94$, Student’s t -test). **D**, The
726 OFT shows that C48/80 treatment reduces the time spent in central zone compared with saline injection (n
727 = 13-14 mice/group, *** $P = 0.0003$; $U = 20$, Mann–Whitney U test). **E**, C48/80 treatment reduces the
728 travel distance on the OFT (*** $P < 0.0001$, $U = 15$, Mann–Whitney U test). **F**, Representative images
729 show the identification of Drd1-MSNs (left) and Drd2-MSNs (right) in coronal NAc slices from Drd1-
730 tdTomato and Drd2-eGFP mice, respectively. **G**, Schematic representation of the experimental schedule
731 and recording site. **H**, A fluorescent-positive neuron was recorded by patch clamp pipette in fluorescent
732 and DIC image modes. **I**, Bar graph and scatter plot for rest membrane potential (RMP) in Drd1-MSNs in
733 slices from the saline-treated and C48/80-treated mice (n = 32-39 neurons/group, * $P = 0.04$, $U = 446.5$,
734 Mann–Whitney U test). **J**, Same as I for rheobase (n = 32-39 neurons/group, * $P = 0.0105$, $t_{69} = 2.631$,
735 Student’s t -test). **K**, Sample traces of action potentials (APs) obtained in Drd1-MSNs in slices from
736 saline-treated and C48/80-treated mice. **L**, The number of evoked action potentials in response to the
737 increasing depolarizing current steps in Drd1-MSNs from saline-treated and C48/80-treated mice
738 ($F_{(\text{interaction } 8, 536)} = 2.384$, $P = 0.0157$; $F_{(\text{treatments } 1, 67)} = 7.241$, ** $P = 0.0090$, two-way ANOVA with repeated
739 measure). **M**, Bar graph and scatter plot for RMP in Drd2-MSNs in slices from the saline-treated (black)
740 and C48/80-treated (green) mice (n = 25-26 neurons/group, $P = 0.6261$, $t_{49} = 0.4903$, Student’s t -test). **N**,
741 Same as M for rheobase (n = 25-26 neurons/group, $P = 0.2363$, $U = 263$, Mann-Whitney U test). **O**,
742 Sample traces of APs obtained in Drd2-MSNs in slices from saline-treated and C48/80-treated mice. **P**,
743 The number of evoked action potentials in response to the increasing depolarizing current steps in Drd2-
744 MSNs from saline-treated and C48/80-treated mice ($F_{(\text{interaction } 8, 384)} = 0.3561$, $P = 0.9428$; $F_{(\text{treatments } 1, 48)} =$
745 4575 , $P = 0.5020$, two-way ANOVA with repeated measure).

746

747 **Figure 2. Chemogenetic activation of Drd1-MSNs in the NAc core decreases C48/80-induced**
748 **scratching behaviors.** **A**, Schematic illustration of virus injection site in the NAc. The AAV-DIO-
749 hm3D(Gq)-mCherry was used for conditional activation of Drd1-MSNs in Drd1-Cre mice. **B**, Schematic
750 diagram of the time line for the experiment. **C**, Representative brain section shows the expression of
751 AAV-DIO-hm3Dq-mCherry in the NAc core. aca, anterior commissure, anterior part. **D**, Viral spread of
752 AAV-DIO-hm3D(Gq)-mCherry and AAV-DIO-mCherry in Drd1-cre mice. Each mouse is represented
753 by one translucent outline, and outlines are overlapped. **E**, Sample traces shows the injected currents-
754 (+100 pA and +140 pA) evoked membrane voltage responses recorded in hm3Dq-expressing Drd1-
755 MSNs before and after CNO (5 μ M) application. Notably, CNO incubating leads a relatively sustained
756 depolarization on the RMP and increases the firing frequency in hm3Dq-expressing cells. **F**,
757 Chemogenetic activation of Drd1-MSNs in the NAc core decreases the scratching behaviors in mice
758 treated with C48/80 ($F_{(\text{interaction } 1, 10)} = 8.282, P = 0.0164$; $F_{(\text{drug } 1, 10)} = 10.16, P = 0.0097$; $F_{(\text{virus } 1, 10)} = 5.298,$
759 $P = 0.041$). **G**, The EPMT shows that chemogenetic activation of Drd1-MSNs in the NAc core does not
760 change the time spent in open arms in mice treated with C48/80 ($F_{(\text{interaction } 1, 10)} = 0.03761, P = 0.8501$;
761 $F_{(\text{drug } 1, 10)} = 0.04718, P = 0.8324$; $F_{(\text{virus } 1, 10)} = 2.805, P = 0.1249$). **H**, Same as G for summary of the open
762 arms entry ($F_{(\text{interaction } 1, 10)} = 1.462, P = 0.2544$; $F_{(\text{drug } 1, 10)} = 0.8845, P = 0.3691$; $F_{(\text{virus } 1, 10)} = 0.6358, P =$
763 0.4438). **I**, The OFT shows that chemogenetic activation of Drd1-MSNs in the NAc core does not change
764 the time spent in central zone in mice treated with C48/80 ($F_{(\text{interaction } 1, 10)} = 0.3991, P = 0.5417$; $F_{(\text{drug } 1, 10)} =$
765 $2.062, P = 0.1816$; $F_{(\text{virus } 1, 10)} = 0.7666, P = 0.4018$). **J**, Same as I for summary of the travel distance
766 ($F_{(\text{interaction } 1, 10)} = 0.01651, P = 0.9003$; $F_{(\text{drug } 1, 10)} = 0.5096, P = 0.4916$; $F_{(\text{virus } 1, 10)} = 3.048, P = 0.1114$).

767

768 **Figure 3. Chemogenetic inhibition of Drd1-MSNs in the NAc core increases C48/80-induced**
769 **scratching behaviors.** **A**, Schematic illustration of virus injection site in the NAc. The AAV-DIO-
770 hm4Di-mCherry was used for conditional suppression of Drd1-MSNs in Drd1-Cre mice. **B**, Schematic
771 diagram of the timeline for the experiment. **C**, Representative brain section shows the expression of

772 AAV-DIO-hM4Di-mCherry in the NAc core. *aca*, anterior commissure, anterior part. **D**, Viral spread of
773 AAV-DIO-hM4D(Gi)-mCherry and AAV-DIO-mCherry in *Drd1-cre* mice. **E**, Sample traces show the
774 injected currents- (+100 pA and +140 pA) evoked membrane voltage responses recorded in hM4Di-
775 expressing *Drd1*-MSNs before and after CNO (5 μ M) application. **F**, Chemogenetic inhibition of *Drd1*-
776 MSNs in the NAc core does not change the scratching behaviors in mice treated with C48/80 at the dose
777 of 100 μ g/50 μ l ($F_{(\text{interaction } 1, 8)} = 1.099$, $P = 0.3251$; $F_{(\text{drug } 1, 8)} = 0.02412$, $P = 0.8804$; $F_{(\text{virus } 1, 8)} = 0.1931$, P
778 $= 0.6719$). **G**, Chemogenetic inhibition of *Drd1*-MSNs in the NAc core enhances the scratching behaviors
779 in mice treated with a lower dose of C48/80 (10 μ g/50 μ l) ($F_{(\text{interaction } 1, 9)} = 8.069$, $P = 0.0194$; $F_{(\text{drug } 1, 9)} =$
780 8.331 , $P = 0.0180$; $F_{(\text{virus } 1, 9)} = 9.858$, $P = 0.0119$). **H**, The EMPT shows that inhibition of *Drd1*-MSNs in
781 the NAc core does not change the time spent in open arms in mice treated with C48/80 (100 μ g) ($F_{(\text{interaction$
782 $_{1,8})} = 0.00156$, $P = 0.9695$; $F_{(\text{drug } 1, 8)} = 0.00156$, $P = 0.09695$; $F_{(\text{virus } 1, 8)} = 1.003$, $P = 0.3459$). **I**, Same as H
783 for the summary of the open arms entry ($F_{(\text{interaction } 1, 8)} = 0.6857$; $P = 0.4316$, $F_{(\text{drug } 1, 8)} = 0.07619$, $P =$
784 0.7895 ; $F_{(\text{virus } 1, 8)} = 2.388$, $P = 0.1608$). **J**, The OFT shows that inhibition of *Drd1*-MSNs in the NAc core
785 does not change the time spent in central zone in mice treated with C48/80 (100 μ g) ($F_{(\text{interaction } 1, 8)} =$
786 0.00249 , $P = 0.9614$; $F_{(\text{drug } 1, 8)} = 1.368$, $P = 0.2757$; $F_{(\text{virus } 1, 8)} = 0.01299$, $P = 0.9121$). **K**, Same as J for
787 summary of the travel distance ($F_{(\text{interaction } 1, 8)} = 0.00036$, $P = 0.9852$; $F_{(\text{drug } 1, 8)} = 0.4664$, $P = 0.5139$; $F_{(\text{virus } 1,$
788 $_{8})} = 0.0117$, $P = 0.9165$). **L**, Same as H for results obtained from mice with a lower dose of C48/80 (10 μ g)
789 treatment ($F_{(\text{interaction } 1, 9)} = 0.6834$, $P = 0.4298$; $F_{(\text{drug } 1, 9)} = 3.33$, $P = 0.1013$; $F_{(\text{virus } 1, 9)} = 4.310$, $P = 0.0677$).
790 **M**, Same as I for the open arms entry ($F_{(\text{interaction } 1, 9)} = 0.9605$, $P = 0.3527$; $F_{(\text{drug } 1, 9)} = 0.4269$, $P = 0.5299$;
791 $F_{(\text{virus } 1, 9)} = 0.04306$, $P = 0.8402$). **N**, Same as J for results obtained from mice with a lower dose of
792 C48/80 treatment ($F_{(\text{interaction } 1, 9)} = 1.951$, $P = 0.1959$; $F_{(\text{drug } 1, 9)} = 0.09541$, $P = 0.7644$; $F_{(\text{virus } 1, 9)} = 1.235$, P
793 $= 0.2952$). **O**, Same as K for the travel distance ($F_{(\text{interaction } 1, 9)} = 1.191$, $P = 0.3035$; $F_{(\text{drug } 1, 9)} = 1.129$, $P =$
794 0.3156 ; $F_{(\text{virus } 1, 9)} = 0.07106$, $P = 0.7958$).
795

796 **Figure 4. C48/80 increases the efficacy of excitatory transmission onto Drd1-MSNs.** **A**, Averaged
797 traces and summary graph of electrical stimuli-evoked EPSCs for Drd1-MSNs from saline-treated and
798 C48/80-treated mice in response to different stimulus intensity (n = 6 neurons/group, $F_{(\text{interaction } 4, 40)} =$
799 3.523 , $P = 0.0148$; $F_{(\text{treatments } 1, 10)} = 14.66$, $**P = 0.0045$, two-way ANOVA with repeated measure). **B**,
800 Averaged traces and summary graph of electrical stimuli-evoked EPSCs for Drd2-MSNs from saline-
801 treated and C48/80-treated mice in response to different stimulus intensity (n = 5-7 neurons/group,
802 $F_{(\text{interaction } 4, 40)} = 0.2464$, $P = 0.9102$; $F_{(\text{treatments } 1, 10)} = 0.01156$, $P = 0.9165$, two-way ANOVA with repeated
803 measure). **C**, Representative traces of sEPSCs obtained in Drd1-MSNs of the NAc core from saline-
804 treated and C48/80-treated mice. **D**, Cumulative probability of sEPSC event amplitude (K-S test, $P =$
805 0.284) for a representative Drd1-MSN. Inset, summary bar graph and scatter plot for sEPSC amplitude in
806 the saline-treated and C48/80-treated mice (n = 12-14 neurons/group, $P = 0.8995$, $U = 81$, Mann-Whitney
807 U test). **E**, Same as D for cumulative probability of interval between sEPSC events (K-S test, $P < 0.0001$)
808 and sEPSC frequency (n = 12-14 neurons/group, $***P < 0.0001$, $t_{24} = 4.858$, Student's t -test). **F**, Sample
809 traces of sEPSCs obtained in Drd2-MSNs. **G**, Cumulative probability of sEPSC event amplitude (K-S test,
810 $P > 0.05$) for Drd2-MSNs. Inset, summary bar graph and scatter plot for sEPSC amplitude in the saline-
811 treated and C48/80-treated mice (n = 10-11 neurons/group, $P = 0.4936$, $t_{19} = 0.698$, Student's t -test). **H**,
812 Same as G for cumulative probability of interval between sEPSC events (K-S test, $P > 0.05$) and sEPSC
813 frequency (n = 10-11 neurons/group, $P = 0.9273$, $t_{19} = 0.09241$, Student's t -test). **I**, Averaged traces and
814 summary graph of PPR for Drd1-MSNs from saline-treated and C48/80-treated mice at different inter-
815 stimulus intervals (n = 8-9 neurons/group, $F_{(\text{interaction } 3, 45)} = 3.488$, $P = 0.0232$; $F_{(\text{treatments } 1, 15)} = 14.66$, $**P =$
816 0.0016 , two-way ANOVA with repeated measure). **J**, Averaged traces and summary graph of PPR for
817 Drd2-MSNs from saline-treated and C48/80-treated mice at different inter-stimulus intervals (n = 8-9
818 neurons/group, $F_{(\text{interaction } 3, 45)} = 0.3581$, $P = 0.7835$, $F_{(\text{treatments } 1, 15)} = 0.1289$, $P = 0.7246$, two-way ANOVA
819 with repeated measure).
820

821 **Figure 5. C48/80 increases the projection from the mPFC to Drd1-MSNs in the NAc core.** **A,**
822 Representative coronal brain slices show the expression of AAV-CaMKII α -Chr2-eYFP in the mPFC,
823 BLA, and vHipp and Chr2-eYFP-containing terminals in the NAc core. aca, anterior commissure,
824 anterior part. **B,** Representative traces of blue LED light-induced action potentials at different frequencies
825 in Chr2-positive neurons in the mPFC. **C,** Blue light-induced EPSC recorded from Drd1-MSN at NAc
826 core in the absence or presence of 20 μ M of DNQX. **D,** Sample traces of light-evoked EPSCs for Drd1-
827 MSN in the NAc core obtained from synapses within the mPFC-to-NAc, BLA-to-NAc, or vHipp-to-NAc
828 pathways in saline-treated and C48/80-treated mice. EPSCs recorded at -70 mV with 50 ms and 100 ms
829 inter-stimulus intervals. Blue lines show the onset of paired light stimulations. **E,** Mean PPR values of
830 Drd1-MSNs obtained from synapses within the mPFC-to-NAc (n = 12-14 neurons), BLA-to-NAc (n =
831 10-13 neurons), or vHipp-to-NAc (n = 11-14 neurons) pathways at different inter-stimulus intervals in
832 saline-treated and C48/80-treated mice ($F_{(\text{interaction } 3, 72)} = 4.872, P = 0.0041$; $F_{(\text{treatments } 1, 24)} = 10.16, P =$
833 0.0040 ; two-way ANOVA with repeated measure). **F,** Sample traces of AMPAR- and NMDAR-EPSCs
834 (left panel of each group) recorded at -70 mV and +40 mV on Drd1-MSNs in the NAc core from the light
835 stimulation of different synaptic inputs in saline- and C48/80-treated mice. Summary bar graph (right
836 panel of each group) shows the AMPAR/NMDAR response ratios on Drd1-MSNs from the different
837 synaptic inputs in saline- and C48/80-treated mice (mPFC input, n = 11-12 neurons; BLA input, n = 10-
838 13 neurons; vHipp input, n = 11-14 neurons).

839
840 **Figure 6. C48/80 increases the excitability of mPFC-to-NAc projection pyramidal neurons.** **A,**
841 Schematic diagram for retrobeads green injection and patch-clamp recording in brain slices. **B,**
842 Representative coronal brain slices show retrobeads injection sites in the NAc core and retrobeads green-
843 positive neurons (green) in the mPFC. aca, anterior commissure, anterior part; NAcC, NAc core; NAcSh,
844 NAc shell. **C,** Images show the electrophysiological recording on retrobeads-labeled pyramidal neurons in
845 the mPFC. Red arrows marked the retrobeads-positive neurons. **D,** Summary bar graph and scatter plot
846 for RMP of green retrobeads-positive PFC-projecting to NAc pyramidal neurons (n = 27-29 neurons, $P =$

847 0.3098, $U = 329$, Mann-Whitney U test). **E**, Same as D for rheobase of pyramidal neurons ($n = 27-29$
848 neurons, $*P = 0.0110$, $U = 244$, Mann-Whitney U test). **F**, Sample traces of membrane voltage responses
849 recorded from green retrobeads-positive PFC-projecting to NAc pyramidal neurons from saline- or
850 C48/80-treated mice. **G**, Summarized data show the number of evoked spikes in the groups as indicated in
851 F ($n = 27-29$ neurons, $F_{(\text{interaction } 8, 400)} = 4.816$, $P < 0.0001$; $F_{(\text{treatments } 1, 50)} = 6.576$, $*P = 0.0134$, two-way
852 ANOVA with repeated measure).

853

854 **Figure 7. Chemogenetic suppression of glutamatergic synaptic afferents from the mPFC to the NAc**
855 **core improves C48/80-induced scratching.** **A**, Schematic illustration of virus injection and the guide
856 cannula implantation. **B**, Schematic diagram of the time line for the experiment. **C**, Representative brain
857 section shows the expression of hm4Di-mCherry in the PFC and hm4Di-mCherry-containing terminals in
858 the NAc core. aca, anterior commissure, anterior part. **D**, Viral spread of AAV-CamKII α -hm4Di-
859 mCherry and AAV-CaMKII α -mCherry in C57Bl/6 mice. **E**, Summary bar graph shows that local
860 microinjections of CNO (1 μM) into the NAc core reduces scratching behaviors evoked by C48/80 ($n =$
861 10-11 mice, $F_{(\text{interaction } 1, 19)} = 36.98$, $P < 0.0001$; $F_{(\text{drug } 1, 19)} = 43.78$, $***P < 0.001$; $F_{(\text{virus } 1, 19)} = 25.08$, $***P <$
862 0.001). **F**, The EPMT shows that inhibition of PFC glutamatergic terminals in the NAc does not change
863 the time spent in open arms in mice treated with C48/80 ($F_{(\text{interaction } 1, 19)} = 2.629$, $P = 0.1214$; $F_{(\text{drug } 1, 19)} =$
864 1.576, $P = 0.2246$; $F_{(\text{virus } 1, 19)} = 0.08392$, $P = 0.7752$). **G**, Same as F for summary of the open arms entries
865 ($F_{(\text{interaction } 1, 19)} = 2.789$, $P = 0.1113$; $F_{(\text{drug } 1, 19)} = 1.513$, $P = 0.2337$; $F_{(\text{virus } 1, 19)} = 0.5778$, $P = 0.4565$). **H**, The
866 OFT shows that inhibition of PFC glutamatergic terminals in the NAc does not change the time spent in
867 central zone in mice treated with C48/80 ($F_{(\text{interaction } 1, 19)} = 4342$, $P = 0.5178$; $F_{(\text{drug } 1, 19)} = 0.08039$, $P =$
868 0.7798; $F_{(\text{virus } 1, 19)} = 2.023$, $P = 0.1712$). **I**, Same as H for summary of the travel distance on the OF
869 ($F_{(\text{interaction } 1, 19)} = 0.2559$, $P = 0.6187$; $F_{(\text{drug } 1, 19)} = 3.341$, $P = 0.0833$).

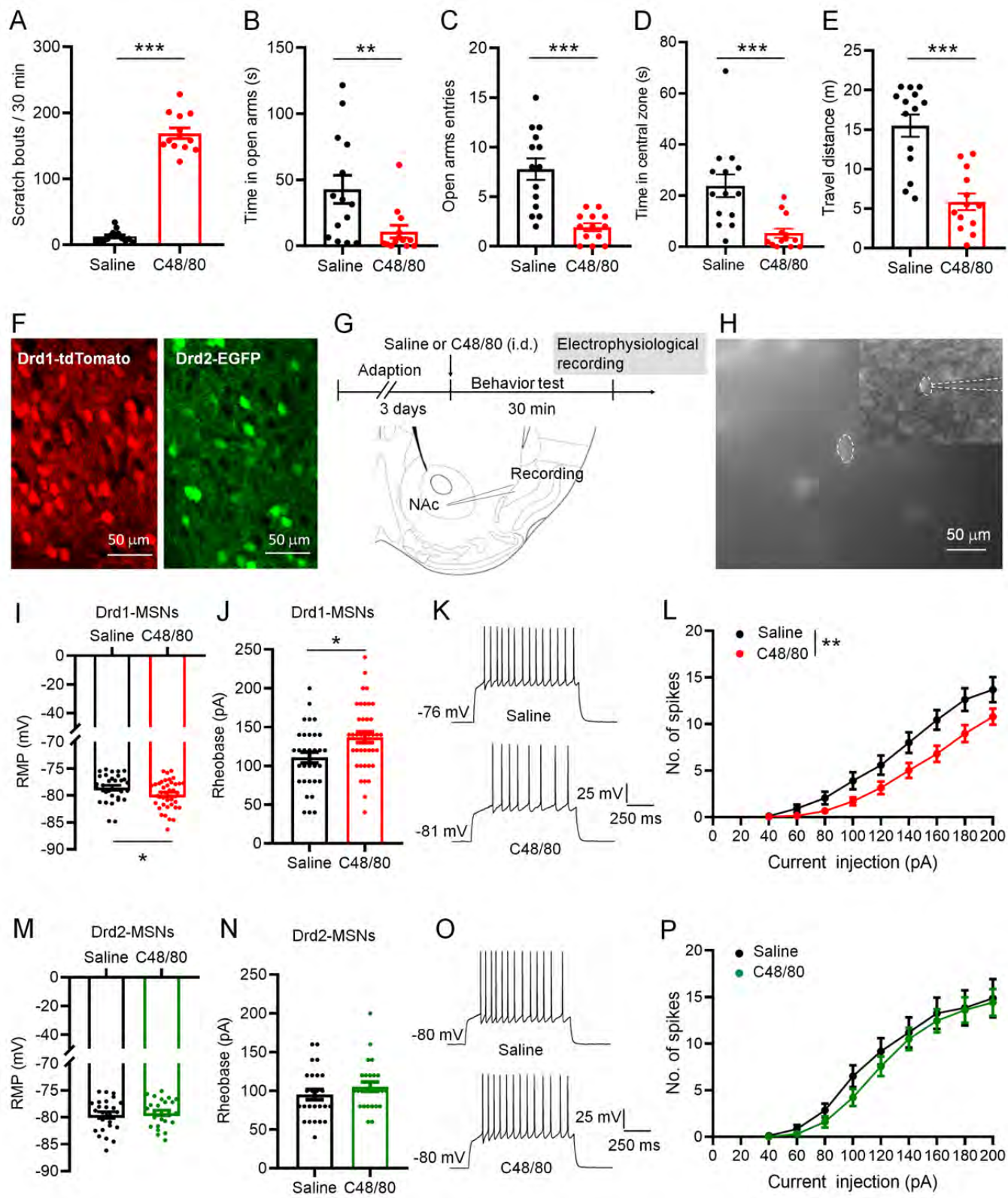
870

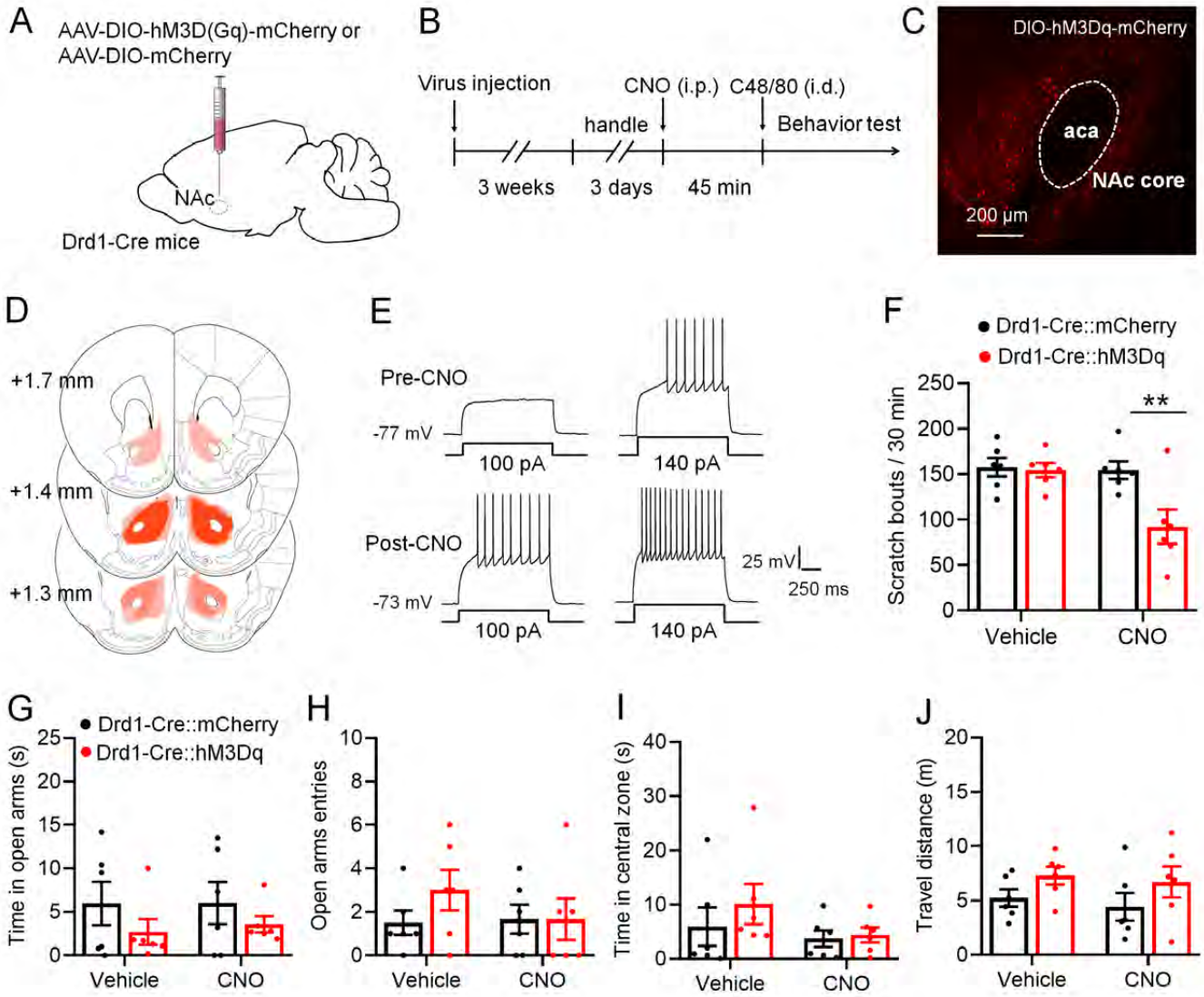
871 **Figure 8. Regulation of KOR in the NAc alters C48/80-induced scratching behaviors. A,**
872 Experimental configuration shows guide cannula implantation in the NAc core. **B,** Schematic diagram of
873 the timeline for the experiment. **C,** Bilateral intra-NAc core infusion of KOR agonist U50488 (0.26
874 $\mu\text{g}/0.3\mu\text{l}$ per side) significantly attenuates C48/80-induced scratching behaviors ($n = 9$ mice for each
875 group, $t_{16} = 3.749$, $P = 0.0018$). **D,** NAc administration of U50488 does not affect the time spent in open
876 arms in mice with treated with C48/80 ($U = 30.50$, $P = 0.3980$). **E,** Same as D for the open arms entry (U
877 $= 35.50$, $P = 0.6853$). **F,** U50488 does not affect the time spent in central zone in mice with treated with
878 C48/80 ($U = 31.50$, $P = 0.4489$). **G,** Same as F for the travel distance ($U = 28$, $P = 0.2973$). **H,** Intra-NAc
879 core pre-infusion of KOR antagonist nor-NBI (0.25 $\mu\text{g}/0.3\mu\text{l}$ per side) increases the low-dose (10 $\mu\text{g}/50\mu\text{l}$)
880 of C48/80-induced scratching behaviors ($n = 12$ to 13 mice for each group, $t_{23} = 2.429$, $P = 0.0234$). **I,**
881 nor-NBI did not affect the time spent in open arms in mice treated with C48/80 (10 μg) ($t_{23} = 0.03014$, P
882 $= 0.9762$). **J,** Same as I for the open arms entry ($U = 57$, $P = 0.2611$). **K,** nor-NBI did not affect the time
883 spent in central zone in mice treated with C48/80 ($U = 65$, $P = 0.4936$). **L,** Same as K for the travel
884 distance ($U = 51$, $P = 0.1519$).

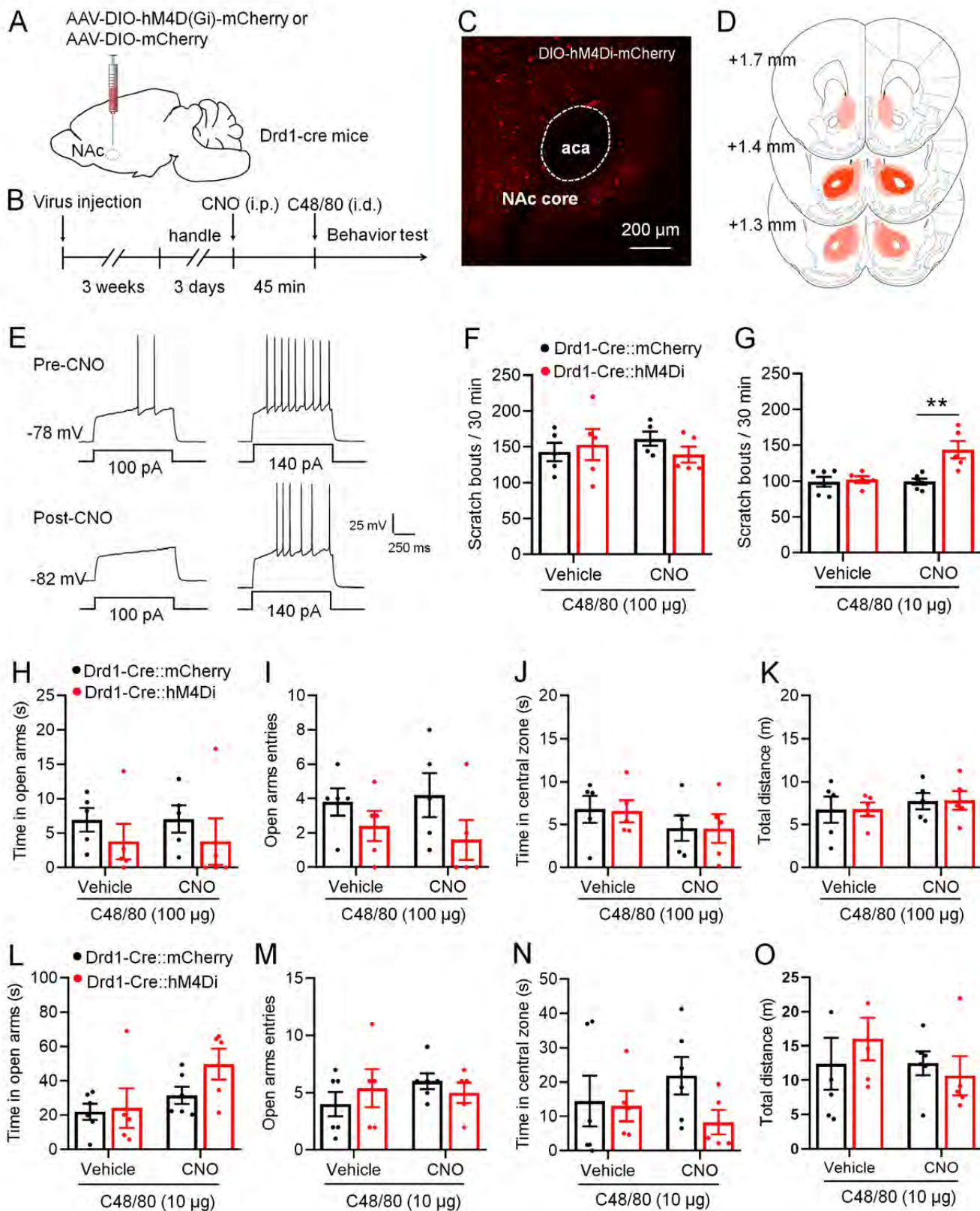
885

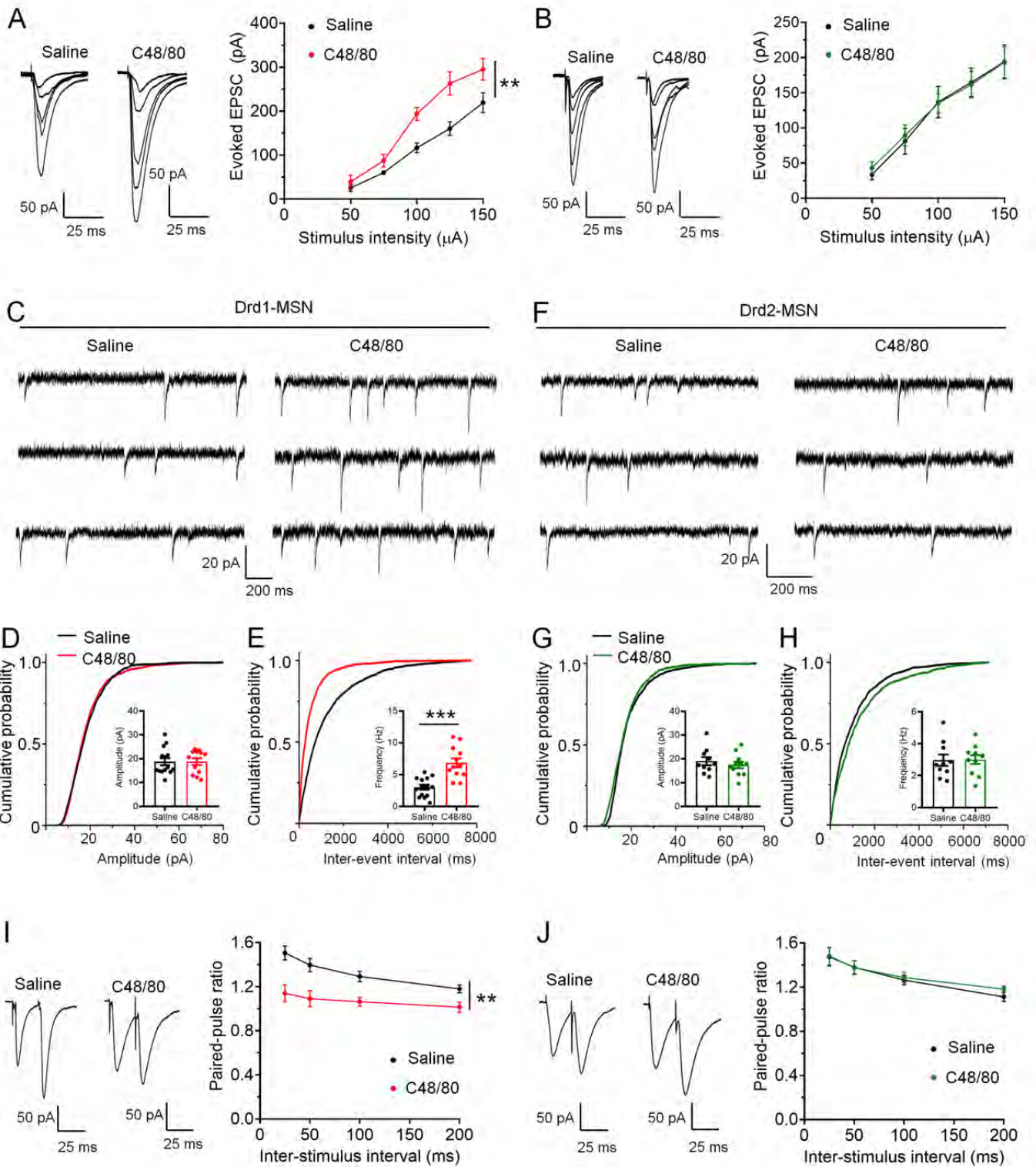
886 **Figure 9. KOR activity changes the frequency of mEPSCs in Drd1-MSNs after C48/80 treatment. A,**
887 Sample traces of mEPSCs recorded in Drd1-MSNs at NAc core from saline- and C48/80-treated mice
888 before and during application of U50488 (1 μM). **B,** Summary of the effects of U50488 on the frequency
889 of mEPSCs recorded from saline and C48/80 treated mice ($n = 7$ -12 neurons, $t_{17} = 2.943$, $P = 0.0091$). **C,**
890 Summary of the effects of U50488 on the amplitude of mEPSCs ($t_{17} = 0.1314$, $P = 0.8970$). **D,** Same as A
891 for mEPSCs obtained in the absence or presence of nor-NBI (0.1 μM) from saline- and C48/80-treated
892 mice. **E,** Summary of the effects of nor-NBI on the frequency of mEPSCs recorded from saline- and
893 C48/80-treated mice ($n = 9$ -11 neurons, $U = 14$, $P = 0.0057$). **F,** Summary of the effects of nor-NBI on the
894 amplitude of mEPSC ($t_{18} = 0.3375$, $P = 0.7396$).

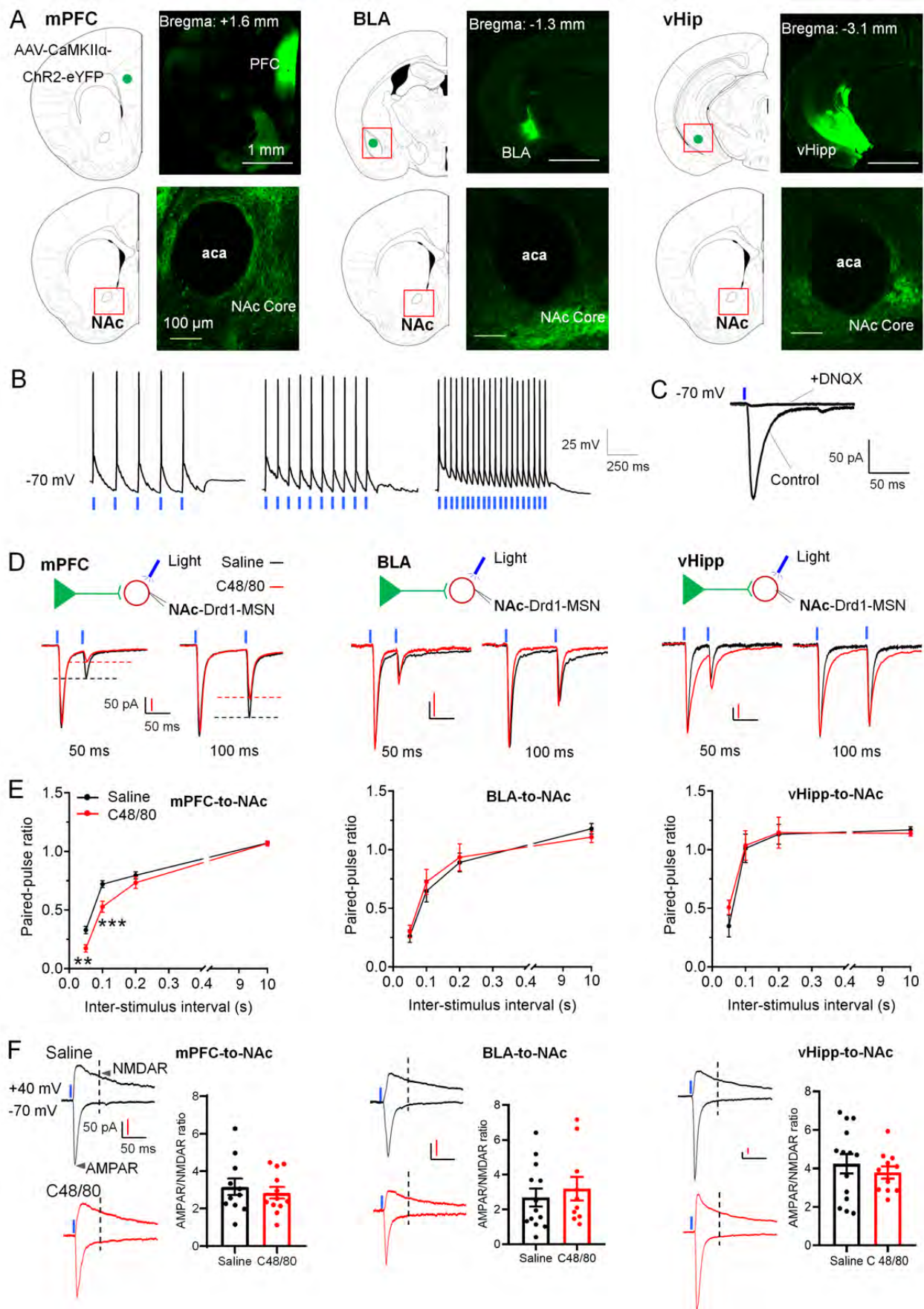
895

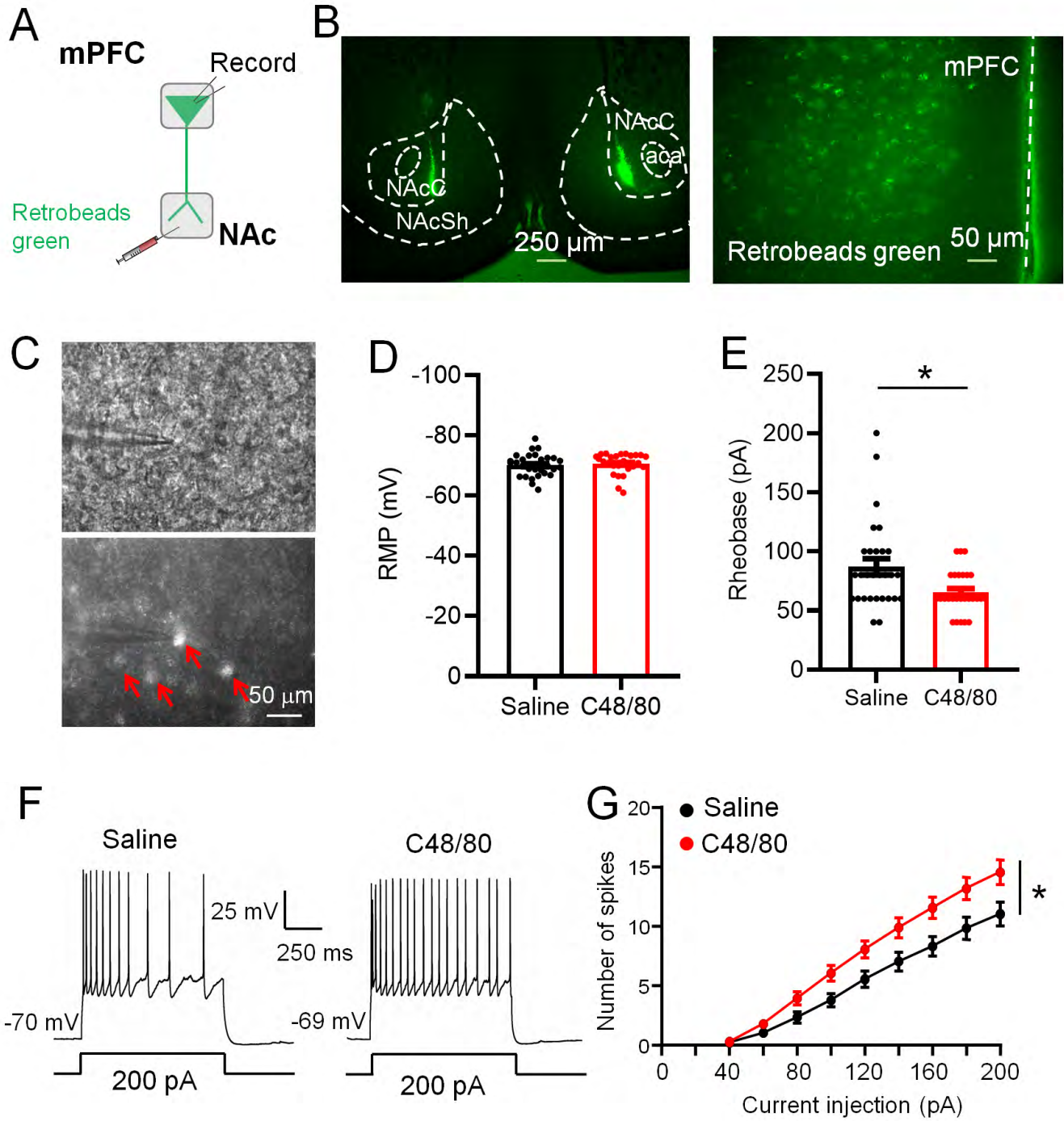




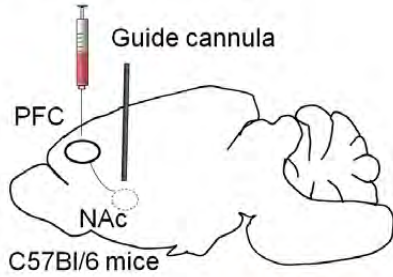




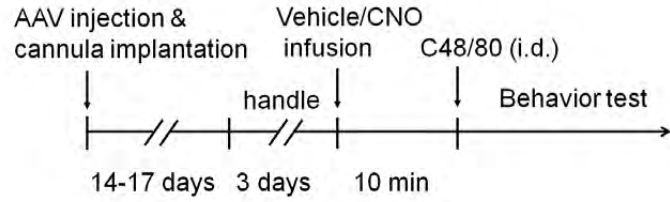




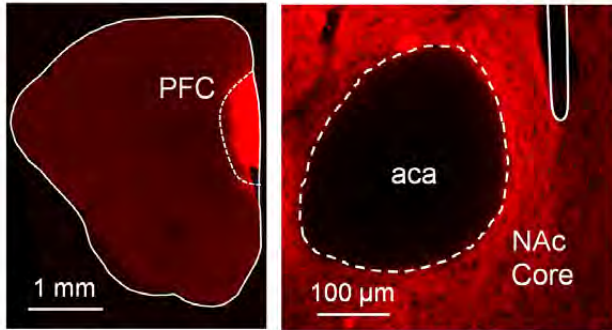
A AAV-CaMKII α -hM4Di-mCherry or AAV-CaMKII α -mCherry



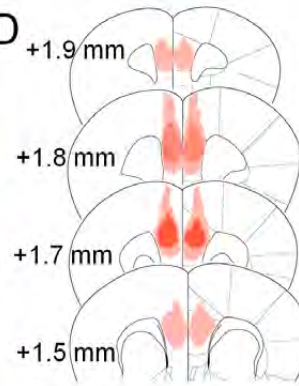
B



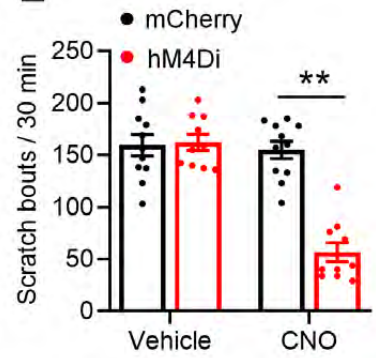
C



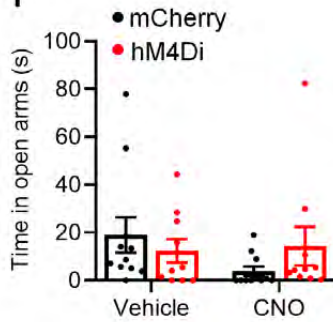
D



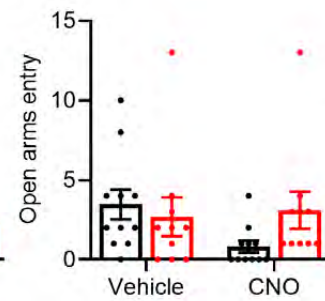
E



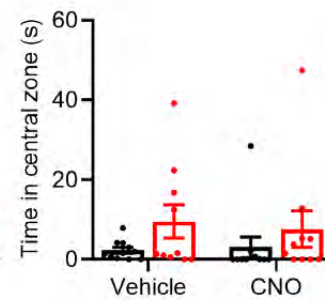
F



G



H



I

